ACS Catalysis

pubs.acs.org/acscatalysis

Research Article

N-Acylethanolamine Acid Amidase (NAAA): Mechanism of Palmitoylethanolamide Hydrolysis Revealed by Mechanistic Simulations

Laura Scalvini, Andrea Ghidini, Alessio Lodola,* Donatella Callegari, Silvia Rivara, Daniele Piomelli, and Marco Mor*

Cite This: *ACS Catal.* 2020, 10, 11797−11813

Read Online

ACCESS | Metrics & More | Article Recommendations | Supporting Information

ABSTRACT: The N-terminal cysteine hydrolase *N*-acylethanolamine acid amidase (NAAA) catalyzes the hydrolytic deactivation of the lipid messenger palmitoylethanolamide (PEA), with optimal activity at acidic pH. Using the crystal structure of human NAAA as a starting point, we investigated the catalytic mechanism of PEA hydrolysis with a multiscale approach based on classic molecular dynamics (MD) and quantum mechanical/molecular mechanics (QM/MM) simulations coupled with enhanced sampling and path-collective variables (PCVs). The proton configuration of the catalytic nucleophile, Cys126, and of the surrounding carboxylates was critical to preserve the active site architecture. A stable Michaelis complex was then used to reconstruct the free-energy surfaces of NAAA acylation and deacylation during PEA hydrolysis. Acylation emerged as the critical step, with Cys126 acting both as an acid, to protonate the ethanolamine leaving group, and as a nucleophile, to attack the PEA carbonyl carbon. The ethanol fragment of PEA did not appear to play an indispensable role in acylation, a result further supported by kinetic experiments showing that NAAA hydrolyzes palmitoyl methyl amide (PMA) with high catalytic efficiency. Our multiscale approach identified a distinctive protonation state and catalytic mechanism for NAAA which accounts for pH-dependent activity, mutagenesis data, and mechanism of covalent inhibitors.

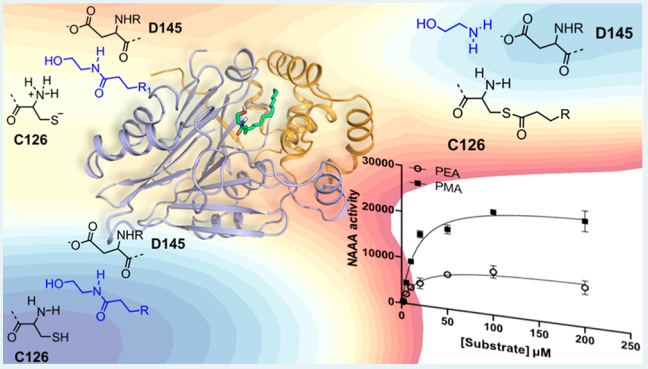

KEYWORDS: *NAAA, palmitoylethanolamide, cysteine, hydrolysis, QM/MM, free-energy surface, path-collective variables*

INTRODUCTION

N-Acylethanolamine acid amidase (NAAA) is a cysteine amidase[1] that, together with fatty acid amide hydrolase (FAAH),[2] contributes to the deactivating cleavage of palmitoylethanolamide (PEA) to palmitic acid and ethanolamine. PEA belongs to a family of bioactive lipid amides known as fatty acid ethanolamides (FAEs),[3] which also includes the endocannabinoid anandamide.[4] PEA has attracted attention because of its analgesic and anti-inflammatory properties,[5] which are due to its ability to bind to and activate peroxisome proliferator-activated receptor-α (PPAR-α).[6,7] Compelling evidence indicates that inflammation is accompanied by a drastic reduction in the levels of PEA in affected tissues;[8] therefore, the development of NAAA inhibitors may represent a novel frontier for the treatment of inflammatory disorders.[9,10]

While NAAA and FAAH share the ability to catalyze the hydrolysis of lipid amides,[11] they differ in nearly every other respect.[12] FAAH is widely expressed in mammalian tissues and is mainly localized in the endoplasmic reticulum and the nucleus. In contrast, NAAA is primarily expressed by immune cells and is localized to acidic organelles such as lysosomes. What is more, NAAA and FAAH share no structural homology. They belong to two distinct superfamilies of amidases and, as such, differ in overall architecture, active site organization, and catalytic properties, including pH dependence and substrate selectivity.[11,12] FAAH is a membrane protein, and it is a member of the amidase signature (AS) superfamily.[13] The active site of FAAH is wide and characterized by three distinct but contiguous cavities which contribute to substrate recruitment and catalysis.[14] FAAH has an uncommon Ser-Ser-Lys catalytic triad, a feature

Received: July 3, 2020
Revised: September 10, 2020
Published: September 15, 2020

https://dx.doi.org/10.1021/acscatal.0c02903
ACS Catal. 2020, 10, 11797−11813

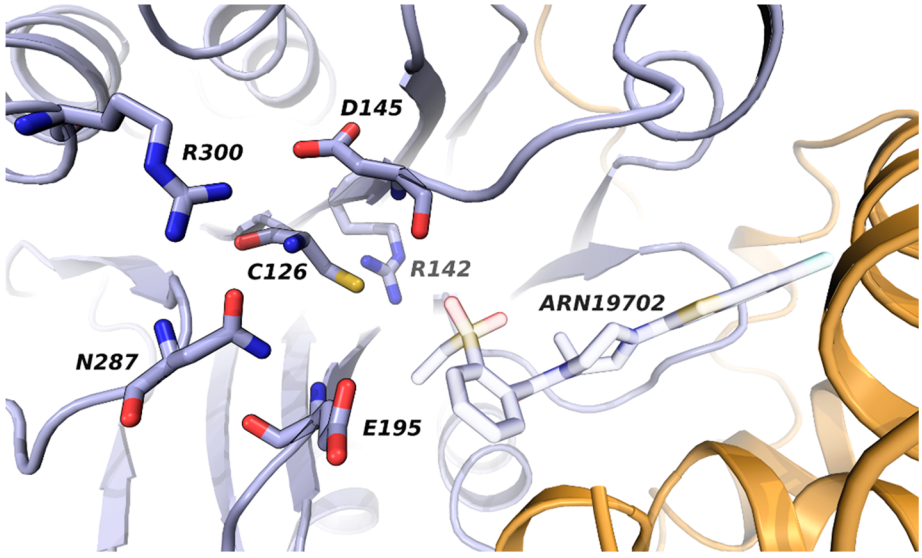

Figure 1. Human NAAA (violet carbon atoms) in a complex with the noncovalent inhibitor ARN19702 (white carbon atoms) as observed in the PDB structure 6DXX.[19] In evidence are Cys126 and other residues of the active site believed to be important in the catalytic cleavage of PEA. The secondary structure of NAAA is displayed in cartoon (gold for the α subunit, violet for the β subunit).

that accounts for its ability to display maximum activity at alkaline pH.[15]

NAAA is a member of the choloylglycine hydrolase family,[1] a subclass of the N-terminal nucleophile hydrolase (Ntn) superfamily,[16] which includes enzymes specialized in the cleavage of linear C−N bonds through their N-terminal cysteine, serine, or threonine residue.[17] NAAA is a soluble protein, and it is produced as an inactive precursor that is processed to a shorter, catalytically competent form by self-cleavage of an internal peptide bond.[18] This reaction is catalyzed by the side chain of the same residue that successively mediates PEA hydrolysis (Cys126 in the human isoform, the numbering of which is adopted in this work; Cys131 in rat NAAA). This maturation process generates a short (α) and a long (β) subunit that remain tightly associated. The β-subunit contains the residues involved in the catalytic cleavage of PEA, while the α-subunit contributes with the β-subunit to the formation of the PEA-binding site.[19]

The substrate-binding site of NAAA is composed of two regions: a narrow lipophilic pocket is deputed to the recognition of the aliphatic tail of PEA, while a solvent-exposed cavity accommodates the ethanolamine head. The diverse organization of the substrate-binding sites of NAAA and FAAH may account for the dissimilar substrate selectivities displayed by these isofunctional enzymes. FAAH has a moderate preference for polyunsaturated long-chain fatty acid amides, such as anandamide (arachidonoylethanolamide), whereas NAAA has a marked preference for saturated substrates.[1] Less is known about the chemical features of the leaving group required to favor an efficient hydrolysis. FAAH, but not NAAA, effectively hydrolyzes *N*-fatty acyl taurines and *N*-fatty acyl glycines,[12] suggesting that the two enzymes may differ in their tolerance for leaving groups of different sizes, shapes, and charges. NAAA possesses low but detectable hydrolytic activity toward ceramides,[1] a class of lipids in which the leaving group is constituted by sphingosine, a bulky amino alcohol which includes in its structure the ethanolamine fragment of PEA.

The crystal structure of the active form of NAAA[19] along with mutagenesis experiments[8,20] have pointed out that, in addition to the N-terminal Cys126, other amino acid residues are important for enzyme activity (Figure 1). These are (i) Arg142 and Asp145 polar endings, which are placed at a hydrogen-bond (H-bond) distance from the sulfhydryl and N-terminal amino group of Cys126, respectively, (ii) the Asn287 side chain and Glu195 NH group, which form the oxyanion hole, and (iii) Arg300, which stabilizes the conformation of the Asn287 side chain through an H-bond and makes electrostatic interactions with the N-terminal amine of Cys126, likely modulating its pK_a. The presence of a large number of ionizable residues in close proximity to the catalytic nucleophile is somewhat uncommon (e.g., in comparison to FAAH) and may account for the ability of NAAA to cleave PEA in the acidic environment of lysosomes, with the maximum activity being reached at pH 4.5.[20] A similar active site composition and architecture are shared by acid ceramidase,[21] another cysteine Ntn-hydrolase with lysosomal distribution.

As first suggested by Oinonen and Rouvinen,[17] Ntn-hydrolase-catalyzed cleavage of an amide may start with deprotonation of the thiol side chain of Cys126 by its own N-terminal amine. Once formed, the thiolate group may attack the amide carbonyl with assistance from the oxyanion hole, which stabilizes the incoming negative charge on the carbonyl oxygen. Expulsion of the amine group results in the formation of a thioester intermediate (acylenzyme), which is readily hydrolyzed to restore the catalytic site. However, while the catalytic mechanism of FAAH has been thoroughly investigated both by experiments[14,15] and with the use of computational approaches,[22] a clear understanding of the details for NAAA catalysis is still lacking, especially in regard to the role played by the acidic amino acid residues surrounding the N-terminal cysteine.

To fill this knowledge gap, we used a set of computational techniques, ranging from classical molecular dynamics (MD) to hybrid QM/MM calculations[23] coupled with enhanced sampling and path-collective variables (PCVs), to identify a probable protonation state for the surroundings of the NAAA catalytic site and to describe at an atomistic level the entire mechanism of PEA hydrolysis, including both acylation and

https://dx.doi.org/10.1021/acscatal.0c02903
ACS Catal. 2020, 10, 11797−11813

deacylation. The results indicate that (i) the protonation of several carboxylate groups in the surroundings of the catalytic Cys126 is critical for model stability, (ii) acylation is a key step in the process of PEA cleavage, and surprisingly, (iii) the terminal hydroxyl group of ethanolamine does not play an essential role in this process. This last finding, which was confirmed by biochemical experiments, suggests that NAAA's substrate selectivity is primarily controlled by the stereoelectronic properties of the fatty acyl portion of the substrate.

METHODS

MD Simulations of NAAA-ARN19702 Complexes with AMBER. Six independent systems (systems **#1**−**#6**) were built attributing alternative protonation states to Cys126, Asp145, and Glu195. For other ionizable groups, the protonation state was assigned on the basis of preliminary MD simulations with the OPLS3e force field,[25] which identified a protonic configuration giving a stable NAAA-ARN19702 complex (system d in section 1 in the Supporting Information, corresponding to system **#3**). In systems **#1**−**#6**, the protein was modeled using the AMBERff15ipq force field,[26] while the ligand (ARN19702) was parametrized using the general AMBER force field (GAFF).[27] TIP3P parameters were applied for the solvent.[28] The molecule of Triton X-100 cocrystallized with NAAA was parametrized using GAFF. The protein−ligand complex was solvated by 16100 TIP3P water molecules, setting an orthorhombic box of 81 Å × 83 Å × 96 Å, and neutralized by adding 11 Cl^- ions.

MD simulations were carried out for 100 ns under NVT conditions at 298 K, after the energy minimization of the system and an equilibration of 15 ns in NVT and 15.5 ns under NPT conditions, using the *pmemd* module of the AMBER16 software.[29] Full electrostatic and van der Waals interactions were computed within a cutoff of 10 Å, and long-range electrostatic interactions were treated using the PME approach. The covalent bonds involving hydrogen atoms were constrained with the SHAKE algorithm, and a time step of 2 fs was applied. Three independent replicas of 100 ns each were performed for each modeled system.

Application of the QM/MM Potential. The NAAA-PEA complex equilibrated with AMBER16 was used for QM/MM calculations.[23] The whole Cys126, the backbone NH group of Thr127, the *N*-(2-hydroxyethyl)propionamide fragment of PEA, and the acetic acid fragments of Asp145 and Glu195 were treated at the QM level with the density functional tight-binding type 3 (DFTB3) approach[30] and represented the reactive region of the system (Figure S4). The resulting QM system was composed of 49 atoms including 4 link atoms, added through the *qmmask* command of AMBER.[29] The default value for the *adjust_q* variable of AMBER ensured that the total charge of the QM, MM, and link portions equaled the original charge applying a charge correction among MM atoms.[29]

All of the other atoms (including solvent molecules) were described with the AMBERff15ipq force field[26] and represented the *nonreactive* region of the system. In the QM/MM approach used here, the effective Hamiltonian of the system is described by eq 1

$$H_{\text{eff}} = H_{\text{QM}} + H_{\text{MM}} + H_{\text{QM/MM}} \quad (1)$$

where H_{QM} is the Hamiltonian of the *reactive region* treated at the DFTB3 level, H_{MM} is the Hamiltonian of the *nonreactive region*, treated with the AMBERff15ipq force field, and $H_{\text{QM/MM}}$ is the Hamiltonian that couples these two regions. A detailed description of the QM/MM approach applied here is described in ref 31.

To maintain the overall architecture of the protein close to the X-ray structure, QM/MM MD simulations (either plain or biased) were performed with application of restraints of 5 kcal mol^{-1} $Å^{-2}$ on the Cα atoms of the protein. However, residues within 5 Å of the catalytic Cys126 were devoid of any restraint to account for the effect of structural fluctuation on the modeled reactions. All of the other atoms of the NAAA-PEA complex (including hydrogens) were free to move. A time step of 0.2 fs was used to integrate the equation of motion. The SHAKE option was turned off during all QM/MM simulations.

QM/MM simulations were performed using the 3OB set of parameters available for DFTB3 calculations. DFTB3/3OB resolves some of the inconsistences reported for earlier versions of the SCC-DFTB approach,[32] including those related to proton transfer reactions involving thiol groups.[33] DFTB3/3OB features high computational efficiency, which made feasible the execution of millions of calculations in a reasonable amount of time. This allowed us to run QM/MM MD simulations for several hundreds of picoseconds, which is critical to reconstruct free energy surfaces for the reactions of interest.[34]

Proton Transfer Reaction Involving Cys126 and Asp145. A snapshot taken from a 400 ps QM/MM MD simulation performed on system **#4** (see the Results) was selected as the starting point for the simulation of the proton transfer reaction. The structure was minimized, with the steepest descent (SD) for 500 steps and then with the conjugate gradient (CG) method, to an energy gradient of 0.005 kcal mol^{-1} $Å^{-1}$ at the DFTB3/AMBER level. The resulting structure was used as an initial geometry for an adiabatic mapping procedure, at the same level of theory, describing the proton transfer from the carboxylic group of Asp145 to the terminal amino group of Cys126 and then to the sulfur atom of Cys126. This process was modeled restraining the system along a complex reaction coordinate defined as a linear combination of the following interatomic distances: $[O_{Asp145}\cdots H_{Asp145}] - [H_{Asp145}\cdots N_{Cys126}] + [N_{Cys126}\cdots H_{Cys126}] - [H_{Cys126}\cdots S_{Cys126}]$. The value of the reaction coordinate ranged from −4.98 to 3.27 Å, divided into 56 windows (step size 0.15 Å). At each grid point, a DFTB3/AMBER minimization (500 steps of SD followed by the CG algorithm) was performed to an energy gradient of 0.005 kcal mol^{-1} $Å^{-1}$ with application of a harmonic restraint of 1000 kcal mol^{-1} $Å^{-2}$ on the reference value of the reaction coordinate. During these minimizations, a torsional restraint was applied on the Asp145 side chain to preserve the polar interaction between the carboxylic group of Asp145 and the N-terminal amine of Cys126.

The geometries obtained after minimization were used as starting points for QM/MM umbrella sampling MD simulations. These were performed by applying a harmonic restraint of 100 kcal mol^{-1} $Å^{-2}$ on the reaction coordinate. Each US simulation window consisted of 45 ps of equilibration, during which the torsional restraint on Asp145 was gradually removed, followed by 350 ps of production dynamics. The weighted histogram analysis method (WHAM)[35] was used to reconstruct the potential of mean force (PMF) by combining the results of each simulation. The geometry of the NAAA-PEA complex at the end of the proton transfer reaction (i.e., with the protonic configuration of system **#3**, with the Cys126 side chain modeled as a thiol and

https://dx.doi.org/10.1021/acscatal.0c02903
ACS Catal. 2020, 10, 11797−11813

Asp145 in carboxylate form) was minimized (500 steps of SD followed by the CG algorithm) to an energy gradient of 0.005 kcal mol $Å^{-1}$ and then subjected to 400 ps of QM/MM MD simulation without any restraint on the reaction coordinate. A snapshot of this configuration was selected as the starting point to model the backward proton transfer reaction (from system **#3** to **#4**), following the same protocol described above.

Acylation (NAAA-PEA Complex). A snapshot taken from the 400 ps QM/MM MD simulation performed on system **#3** was selected as the starting point for the acylation reaction. The starting structure was minimized (500 steps of SD followed by the CG algorithm) to an energy gradient of 0.005 kcal mol^{-1} $Å^{-1}$ at the DFTB3/AMBER level and used as the initial geometries for adiabatic mapping simulations aimed at transforming the NAAA-PEA Michaelis complex into the acylenzyme. This process was simulated using two distinct reaction coordinates. The first, named Rx and describing the nucleophilic attack by Cys126 to the carbonyl carbon of PEA and elimination of the leaving group, was defined by the linear combination of the following interatomic distances: $[N_{PEA}\cdots C_{PEA}] - [C_{PEA}\cdots S_{Cys126}]$. The second coordinate, Ry, described the proton transfer from the nucleophile Cys126 to the nitrogen atom of the leaving group, and it was defined as $[S_{Cys126}\cdots H_{Cys126}] - [H_{Cys126}\cdots N_{PEA}]$. The value of Rx ranged from −1.93 to 0.77 Å, with a step size of 0.15 Å, while Ry ranged from −1.57 to 2.23 Å, with a step size of 0.20 Å. At each grid point a DFTB3/AMBER level minimization (500 steps of SD followed by the CG algorithm) was performed to an energy gradient of 0.005 kcal mol^{-1} $Å^{-1}$ by application of a harmonic restraint of 1000 kcal mol^{-1} $Å^{-2}$ on the reference value of the reaction coordinate. From this procedure, a potential energy surface was also obtained. Each minimized structure obtained from the adiabatic mapping was used as a starting point for the QM/MM umbrella sampling MD simulations. In this case, harmonic restraints of 100 kcal mol^{-1} $Å^{-2}$ were applied on the reaction coordinates. Each simulation window consisted of 45 ps of QM/MM US equilibration, followed by 60 ps of QM/MM US production. PMF was obtained using the WHAM 2-D approach,[36] including in the calculations only the production phase of each simulated window. The minimum free energy path on the surfaces was determined using MEPSA software (see the Supporting Information for details).[37]

Deacylation: Model Building and QM/MM Simulations. To generate a starting point for the deacylation reaction, a snapshot of the acylenzyme system was extracted from the QM/MM umbrella sampling simulations of the acylation reaction for the NAAA-PEA complex. The thioester fragment (composed of a Cys126 backbone and a Cys126 side chain covalently bound to the palmitic acid chain), the ethanolamine molecule, and the Triton X-100 residue were parametrized with GAFF,[27] while all of the other atoms were treated with the AMBERff15ipq force field.[26]

The geometry of the acylenzyme was minimized without any restraint on the reaction coordinates to an energy gradient of 0.005 kcal mol^{-1} $Å^{-1}$ and was equilibrated for 10 ns by an MM MD simulation using AMBER. The ethanolamine molecule was then removed, and 200 ps of an MM simulation in the NPT ensemble, with restraints of 5 kcal mol^{-1} $Å^{-2}$ on the heavy atoms of the protein and PEA, was performed to favor the equilibration of the solvent box. The *reactive region* was modified, removing the ethanolamine from the QM system while a water molecule was added. The resulting QM region was composed of 41 atoms including 4 link atoms. The system was then subjected to 1 ns of QM/MM simulation. A representative snapshot, using a water molecule situated within 3 Å of the carbonyl carbon of the acylenzyme and undertaking polar contacts with the amino group of Cys126 and with the oxygen atom of Asp145 backbone, was selected as the starting point for the deacylation reaction. The starting structure was thus minimized to an energy gradient of 0.005 kcal mol^{-1} $Å^{-1}$ and provided the initial geometries for DFTB3/AMBER adiabatic mapping.

The deacylation process was simulated using two reaction coordinates. The first one, Rs, described the nucleophilic attack of the water molecule and the breakage of the thioester bond and was defined as a linear combination of the following interatomic distances: $[S_{Cys126}\cdots C_{PEA}] - [C_{PEA}\cdots O_{WAT}]$. The second coordinate, Rt, described the proton transfer from the nucleophile water to the amino group of Cys126 and was defined as $[O_{WAT}\cdots H_{WAT}] - [H_{WAT}\cdots N_{PEA}]$. The value of Rs ranged from −1.09 to 1.51 Å, with a step size of 0.1 Å, while the value of Rt ranged from −0.91 to 0.89 Å, with a step size of 0.15 Å. At each grid point, a DFTB3/AMBER level minimization (500 steps of SD followed by the CG algorithm) was performed to an energy gradient of 0.005 kcal mol^{-1} $Å^{-1}$ with application of a harmonic restraint of 1000 kcal mol^{-1} $Å^{-2}$ on the reference value of the reaction coordinate. From this procedure, a potential energy surface was also calculated. Each minimized structure obtained from the adiabatic mapping was used as a starting point for QM/MM umbrella sampling MD simulations. In this case, harmonic restraints of 100 kcal mol^{-1} $Å^{-2}$ were applied on the reaction coordinates. Each simulation window consisted of 45 ps of QM/MM US equilibration, followed by 60 ps of QM/MM US production. PMF was obtained using the WHAM 2-D approach,[35,36] including in the calculations only the production phase of each simulated window. The minimum free energy path on the surfaces was determined using MEPSA software (see the Supporting Information for details).[37]

Generation of rNAAA-Overexpressing HEK-293 Cells. The encoding sequence of rat NAAA (BC105771) was amplified from the cDNA clone 7930474 (Open Biosystems) using the following primer pair: the forward primer 5′-CCCAAGCTTATGGGGACCCCAGCCATCCG (the *Hin*dIII restriction site is underlined) and the reverse primer 5′-CCGCTCGAGTCA**ATGATGATGATGATGATG**GCTTGGGTTTCTGATC (the XhoI restriction site is underlined). A (6x)-histidine tag was introduced in the reverse primer sequence (highlighted in boldface). The PCR product was cloned into the pCDNA 3.1 vector (Invitrogen) using *Hin*dIII and XhoI restriction enzymes (New England Biolabs). HEK-293 cells (American Type Culture Collection) were cultured at 37 °C in an incubator (5% CO_2) using complete Dulbecco's modified Eagle's medium (DMEM) containing 10% fetal bovine serum (FBS), 1% penicillin−streptomycin, and 1% L-glutamine and transfected with the rat NAAA(6xHis)-pCDNA3.1 construct using the JetPEI transfection reagent (Polyplus), following the manufacturer's instructions. Stably transfected cells were selected by the addition of G418 (1 mg mL^{-1}) to the cell culture medium, and cell clones were generated by limiting dilution plating. Growing clones were analyzed for NAAA expression by Western blot (anti-hASAHL, R&D Systems).

Lysosomal Extract Preparation. HEK-293 cell pellets were resuspended in Tris-HCl buffer (50 mM) containing

https://dx.doi.org/10.1021/acscatal.0c02903
ACS Catal. 2020, 10, 11797−11813

sucrose (0.32 M, pH 7.4). Samples were sonicated with a Branson 102C digital Sonifier. Samples were centrifuged at 800*g* for 15 min at 4 °C, and the resulting supernatants were centrifuged at 12000*g* for 30 min at 4 °C. The pellets were suspended in PBS (pH 7.4) and subjected to two freeze/thaw cycles at −80 °C. The suspension was centrifuged at 100000*g* for 1h at 4 °C. The protein concentration was measured, and samples were stored at −80 °C until use.

NAAA Activity Assay. The substrates PEA and palmitoyl methyl amide (PMA) were prepared at >95% purity, following standard procedures (see the Supporting Information). Substrates were incubated in 100 mM NaH_2PO_4, 100 mM sodium citrate, 0.1% Triton-X 100, 3 mM DTT, at pH 4.5 (NAAA assay buffer) with 4 μg of lysosomal extract protein at 37 °C for 30 min (triplicate samples). Reactions were terminated by addition of 0.6 mL of a cold mixture of methanol and chloroform (1/1) containing *Z*-10-heptadecenoic acid (12.5 ng/mL, Cayman Chemical, Ann Arbor, MI) as an internal standard. Samples were centrifuged (3000 rpm, 15 min, 4 °C), the organic phases were transferred into new vials and dried, and the residues were dissolved in 0.3 mL of methanol/chloroform (9/1, v/v). Analyses were carried out by liquid chromatography/mass spectrometry (LC/MS) using an Agilent 6410 Triple Quad LC/MS system (Agilent Technologies, Wilmington, DE). Palmitic and heptadecenoic acids were eluted from a Zorbax Eclipse XBD-C18 column (2.1 × 50 mm, 1.8 μm pore size, Agilent Technologies, Wilmington, DE) at 0.4 mL/min for 6 min with a solvent mixture of water (A) and methanol (B), both containing 0.25% acetic acid and 5 mM ammonium acetate (0−2 min 90% B, 2−3 min 95% B, 3−6 min 90% B). The column temperature was set at 40 °C. Electrospray ionization was in the negative mode, and the capillary voltage was 4 kV. N_2 was used as the drying gas at a flow rate of 13 L/min and a temperature of 350 °C. The $[M - H]^-$ ion was monitored in the selected-ion monitoring mode (m/z: palmitic acid 269.3, heptadecenoic acid 267.3). Calibration curves were generated using commercial heptadecenoic acid (Cayman Chemical, Ann Arbor, MI) and palmitic acid (Nu-Chek Prep Inc., Elysian, MN). The NAAA activity was calculated as pmol of palmitic acid produced by 1 mg of NAAA in 1 min. Activity data were plotted as a function of the substrate concentration, and K_m and V_{max} values were calculated using a Michaelis−Menten function analysis on GraphPad Prism version 8.4.2 (GraphPad Software Inc.). A comparison with the activity of lysosomal extracts from HEK-293 cells that did not express NAAA (Figure S23 in the Supporting Information) showed that, under the conditions of our assay, approximately 90% of PEA hydrolysis can be ascribed to NAAA activity.

RESULTS

Protonation State and Structural Stability of NAAA Catalytic Site. Our computational investigations started from the structure of human NAAA (hNAAA) in a complex with the noncovalent inhibitor ARN19702 (PDB code 6DXX, Figure 1).[19] The selection of this complex was driven by the observation that ARN19702 does not directly contact catalytic Cys126, whereas in other available structures this residue is variously perturbed. We first evaluated the dynamic stability of the model by performing MD simulations using two different force fields and building systems with different configurations at ionizable groups surrounding the catalytic site (see Methods and the Supporting Information). Automatic assignments of ionic states to weakly acidic or basic groups, based on the preparation module of the Schrödinger 2018-2 suite or on the pK_a values estimated by the program PropKa[38] (Table S1 in the Supporting Information) yielded unstable models in which interactions among key amino acid residues (Cys126, Arg142, Asp145, Asn287, and Arg300) were lost during the first ns of simulation. We thus adjusted the protonation state of ionizable groups surrounding the catalytic site to identify a protonic configuration of NAAA consistent with its structural organization. In doing this, we considered that NAAA's hydrolytic activity is very low at neutral pH and is a maximum between pH 4 and 5.[20] In a first set of simulations performed with the OPLS3e force field[25] (see the Supporting Information), different combinations of protonation states were assigned to the carboxylate groups surrounding the catalytic cavity (see Table S2), while the catalytic cysteine was modeled both in its neutral form (NH_2/SH) and in its positively charged form (NH_3^+/SH). We found that only a specific pattern of protonation allows the conservation of the catalytic site geometry, with Cys126 close to Asp145 and Arg300, and of the expected conformation of Asn287 for the oxyanion-hole structure during MD simulations (see Figures S1−S3 in the Supporting Information). In particular, a stable NAAA-ARN19702 complex was obtained only when Cys126 was modeled in neutral form, Asp194, Glu195, Glu297 ,and Asp200 as neutral carboxylic acids, and Asp145, Asp197, and Asp298 as anionic carboxylates.

The protonation state of peripheral groups giving a stable NAAA-ARN19702 complex with the OPLS3e force field was retained in a second set of MD simulations, where we applied the AMBER force field. At this stage, we focused on the protonation state of the catalytic cysteine and of its closer surroundings. Two residues, Asp145 and Glu195, needed special attention owing to their potential role in catalysis.[8,20] We initially assumed that under mildly acidic conditions the terminal amine of Cys126 is protonated and forms a salt bridge with the carboxylate anion of Asp145. In this configuration (labeled **#1** in Figure 2), the thiol and carboxylic groups of Cys126 and Glu195 were modeled as neutral. System **#1** has been proposed to be catalytically active in the case of acid ceramidase,[21] and this is supported by PropKa software.[38] (see Table S1 in the Supporting Information).

An MD simulation of system **#1** evidences structural instability of the NAAA active site, as shown by the wide fluctuation in the position of the heavy atoms of most of the residues important for catalysis, quantified in terms of root-mean-squared deviation (RMSD) with respect to the coordinates of the X-ray structure (Figure 3 and Figure S5 in the Supporting Information) or in terms of the root-mean-squared fluctuation (RMSF) (Figure S6 in the Supporting Information). This instability is apparently due to the electrostatic repulsion between the positively charged N-terminal amino group of Cys126 and the guanidium group of Arg300. Such a repulsion not only causes significant variation in the position of the catalytic cysteine but also determines a major rearrangement of Arg300, which eventually leads to the breakage of the H-bond with Asn287, disrupting the oxyanion-hole architecture.

We tested an alternative protonation state (**#2**) where a proton was shifted from the N-terminal amino group of Cys126 to the side chain of Asp145. As for system **#1**, MD simulations show large fluctuations in the positions of Cys126, Asp145, and Arg300 and a substantial rearrangement of the

https://dx.doi.org/10.1021/acscatal.0c02903
ACS Catal. 2020, 10, 11797−11813

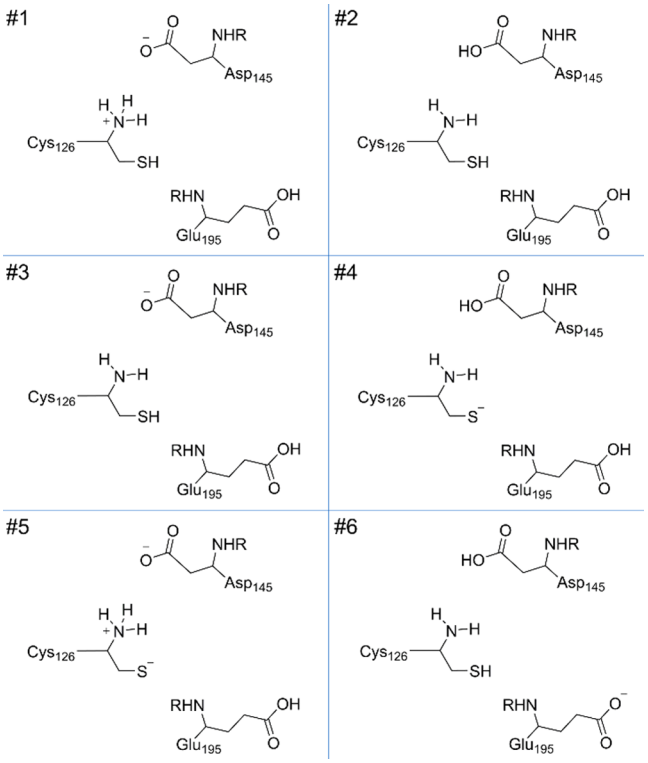

Figure 2. Protonation states for the critical residue of NAAA considered in the present study.

active site (Figure 3 and Figures S5 and S6 in the Supporting Information). We thus explored configurations containing one less proton and performed MD simulations for a model with Asp145 in the anionic form and Cys126 in the neutral state (**#3**) and for its tautomer having a neutral Asp145 carboxylic acid and a Cys126 amino group, while the Cys126 thiolate was anionic (**#4**). Limited fluctuations of the NAAA active site are observed for both systems **#3** and **#4** (Figure 3 and Figures S5 and S6 in the Supporting Information), with all of the elements of the catalytic machinery maintaining for at least 100 ns a conformation resembling that observed in the X-ray structure. It is worth noting that system **#4** slightly outperforms **#3**, which displays a higher mobility in the position of Asp145 (Figure S5 in the Supporting Information). We then investigated if other configurations in equilibrium with system **#4** could give stable structures during MD simulations. In system **#5**, a proton was moved from Asp145 to the N-terminal amine of Cys126, giving a zwitterionic cysteine and an ionized Asp145, while in system **#6**, the carboxylic proton of Glu195 was moved to the Cys126 thiolate, to yield a neutral cysteine and an ionized Glu195. Again, the presence of a protonated N-terminal amine has a negative effect on the structural stability of Cys126, which shows significant fluctuations in comparison to X-ray coordinates or to system **#4** (Figure 3). In **#6**, the presence of Glu195 in an anionic form has a dramatic effect on the NAAA structure, compromising the overall architecture of the active site (Figure 3 and Figures S5 and S6 in the Supporting Information). The active site collapse is triggered by Glu195 that, following a change in its side chain conformation, places the carboxylate group in the oxyanion hole repelling Asn287. These MD simulations point to system **#4** as being the most consistent with the structure of the NAAA active site.

NAAA−PEA Complex. Starting from the protonic configuration **#4**, we built a three-dimensional model of the Michaelis complex by docking PEA into the active site of NAAA (see the Supporting Information for details). The resulting complex (Figure 4A) is similar to that recently described by Gorelik et al.,[19] with the aliphatic chain of PEA laying in the same hydrophobic cavity occupied by myristic acid in a complex with rabbit NAAA (Figure S7 in the Supporting Information) and with the amide group close to the sulfur atom of Cys126. In this arrangement, the amide group forms a polar interaction with the backbone carbonyl oxygen of Asp145 and two H-bonds with the oxyanion hole, one with the backbone NH group of Glu195 and the other with the amide side chain of Asn287. The terminal hydroxyl group of the ethanolamine moiety is placed in a calix-shaped cavity lined by Asp145, Asn287, and Glu195.

This system was submitted to MD simulations using the AMBER force field (see the Supporting Information for details). Three 100 ns long replicates were performed, in which the catalytic site maintains an arrangement similar to that

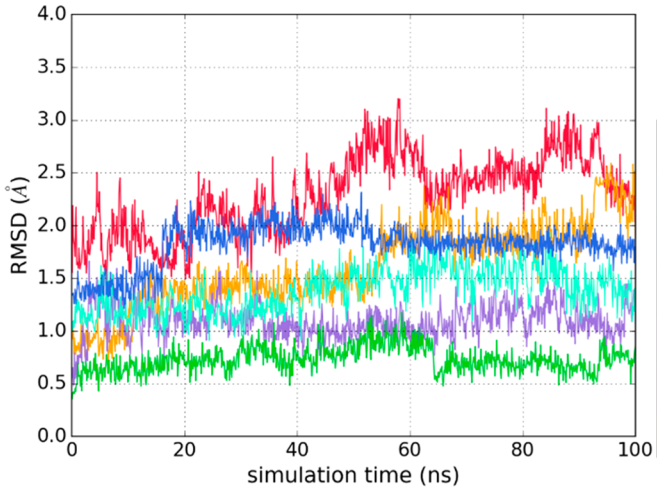

	C126			
Sys.	Nter	chain	D145	E195
#1	+1	0	-1	0
#2	0	0	0	0
#3	0	0	-1	0
#4	0	-1	0	0
#5	+1	-1	-1	0
#6	0	0	0	-1

Figure 3. Analysis of the average RMSD of the heavy atoms of the residues shaping the active site of NAAA (Cys126, Asp145, Glu195, Asn287, and Arg300). The average RMSD was calculated for each of the six independent runs of MD simulations performed, starting from a different protonic configuration of the active site (table on the right; see also Figure 2). The table reports the net charge of Cys126, Asp145, and Glu195.

https://dx.doi.org/10.1021/acscatal.0c02903
ACS Catal. 2020, 10, 11797−11813

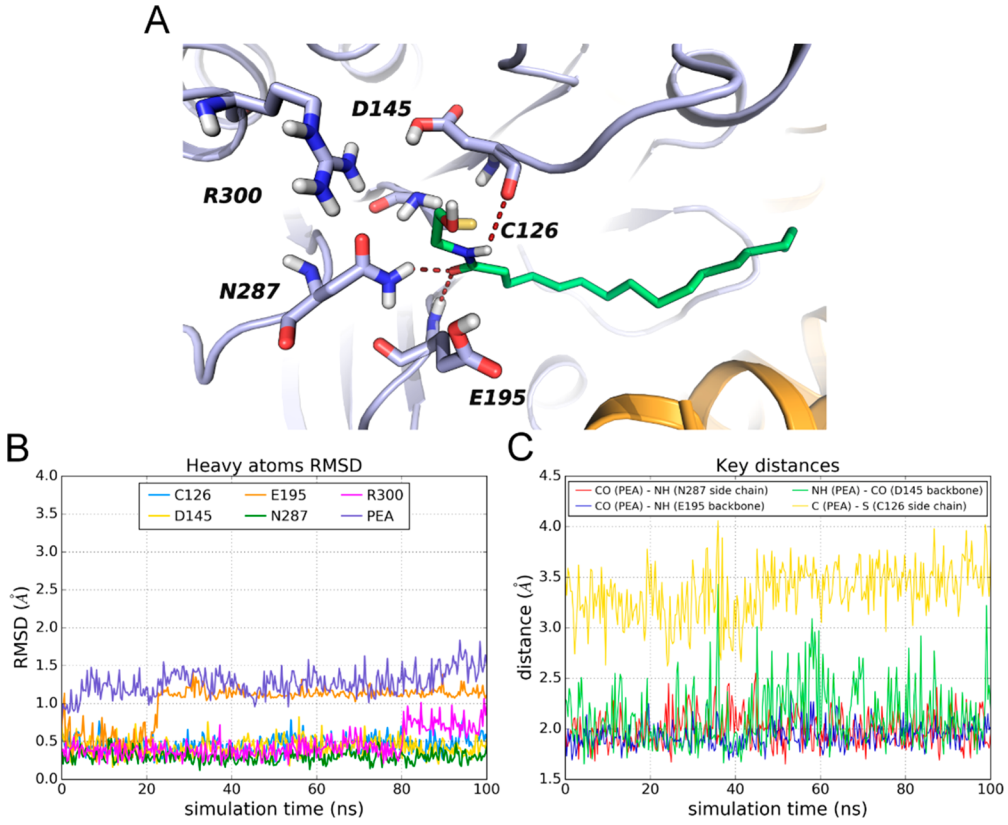

Figure 4. (A) Docking pose of PEA (green carbon atoms) within the NAAA catalytic site (violet carbon atoms). Cys126 and other residues involved in the recognition of the amide portion of PEA are shown, with hydrogen bonds between the amide and the enzyme evidenced as dashed lines. The secondary structure of NAAA is displayed in cartoon form (gold for the α subunit and violet for the β subunit). (B) RMSD analysis for the heavy atoms of residues shaping the active site cleft of NAAA, namely Cys126, Asp145, Glu195, Asn287, and Arg300, during an MD simulation. (C) Evolution during the MD simulation of interatomic distances between the NH groups of Glu195 and Asn287 and the carbonyl oxygen of PEA, the backbone carbonyl of Asp145, and the amide hydrogen of PEA and between the sulfur of Cys126 and the carbonyl carbon of PEA.

observed in the crystal structure (Figure 4B). None of the key residues shows an RMSD variation significantly higher than 1.5 Å. PEA moderately oscillates around its docked conformation (average RMSD of 1.05 ± 0.18 Å) and maintains H-bonds with oxyanion residues, with distances of 1.93(±0.12) and 1.99(±0.17) Å for the interaction between the PEA carbonyl oxygen and the NH of Glu195 or amide NH of Asn287, respectively (Figure 4C). The interaction between the backbone oxygen of Asp145 and amide NH of PEA is also preserved, with a distance of 2.12(±0.31) Å (Figure 4C). This network of interactions allows the sulfur atom of Cys126 to be kept at a distance of only 3.48(±0.45) Å from the carbonyl carbon of PEA. Differently from the amide group, the ethanolamine hydroxyl does not find a specific interactor, as it alternatively undertakes H-bonds with the Asp145 backbone oxygen or with the side chain carboxylic oxygen of Asn287 and Glu195 (Figure S8 in the Supporting Information).

On the other hand, at simulation times higher than 10 ns, some movements of the peripheral helices α3 and α6, which are associated with tensioactive molecules in the crystal structures,[19] were observed. Given the stability of the catalytic site and its surroundings, we concluded that crystallographic structures of this portion represent the solution structures well. To avoid long-range rearrangements of the protein, we introduced positional restraints to the Cα of peripheral regions in the following QM/MM simulations.

Prototropic Equilibria Involving Cys126 and Asp145 by QM/MM Simulations. We next used hybrid QM/MM simulations in combination with umbrella sampling (US) and the WHAM approach[35] to determine the predominant protonation state of Cys126 and Asp145 in the presence of PEA. We focused our attention on configurations **#3** and **#4** (Figure 2), which gave stable MD simulations. We thus calculated the potential of mean force (PMF) for two consecutive reactions transforming configuration **#4** to **#3** (see Methods), moving a proton from the carboxylic acid group of Asp145 to the N-terminal amine of Cys126 and thus generating the intermediate configuration **#5** and then moving another proton from the N-terminal ammonium group to the sulfur atom of Cys126. The complex reaction coordinate (RC) was the combination of four interatomic distances (see Figure 5) free to change individually. Its progress from negative to positive values caused at first the proton exchange from the carboxylic group of Asp145 to the amine, at RC values between −2.5 and −2.4 Å, and then the transfer of another proton from the amine to the thiolate group, at RC values between 1.0 and 1.1 Å. The changes in single interatomic distances show that the two proton transfers occur progressively without recrossing during the RC progress (Figure S9 in the Supporting Information).

The PMF reported in Figure 5 indicates that **#3** is more stable than **#4** by nearly 3.5 kcal mol^{-1}. Configuration **#3** is also more stable than **#5** by 3.0 kcal mol^{-1}, thus emerging as the energetically preferred protonic configuration of the NAAA-PEA complex at the DFTB3/AMBER level. The evolution of the PMF as a function of the time of simulation

https://dx.doi.org/10.1021/acscatal.0c02903
ACS Catal. 2020, 10, 11797−11813

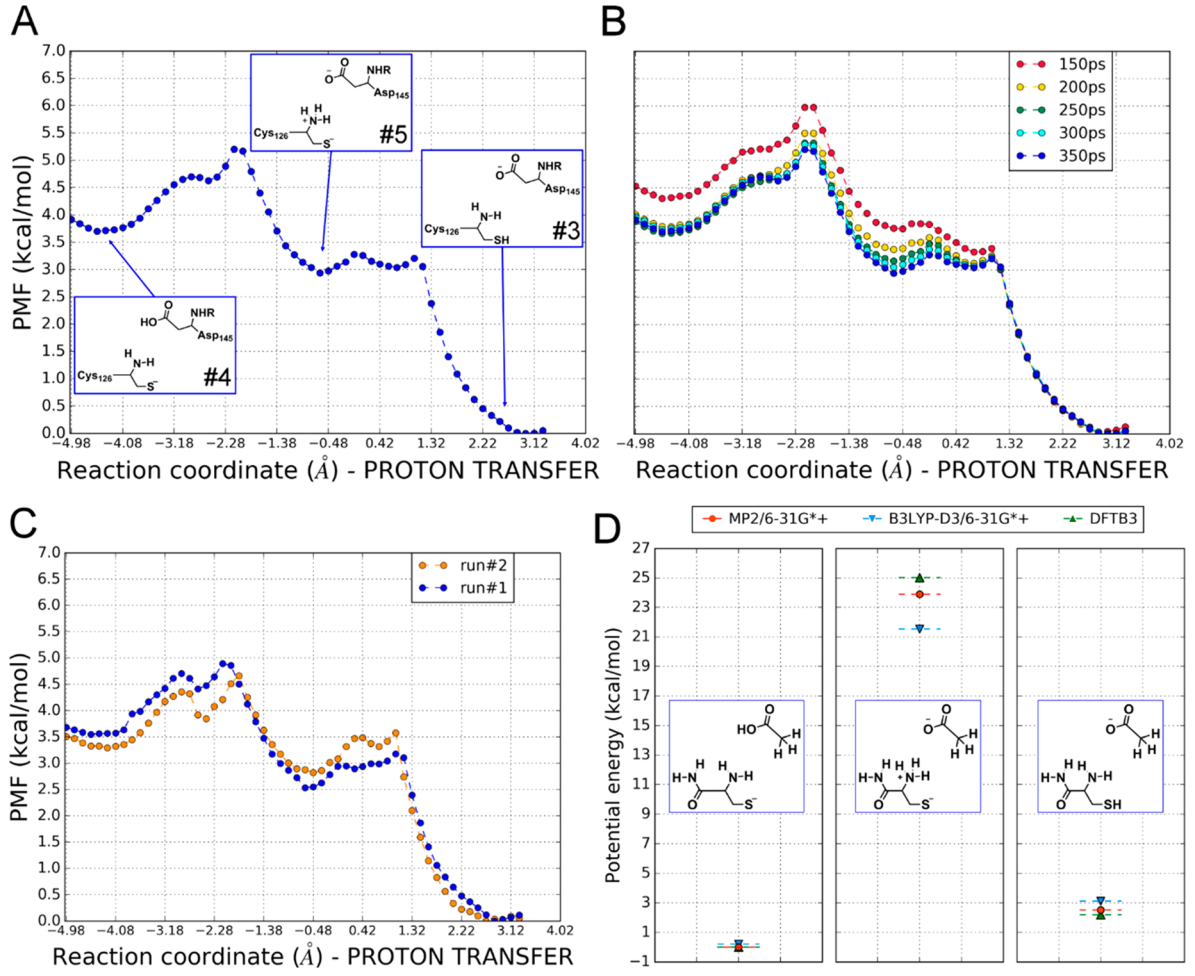

Figure 5. (A) Proton transfer reaction connecting configuration **#4** to configuration **#3**. PMF is given in kcal mol^{-1}, and the reaction coordinate, defined as $[O_{Asp145}\cdots H_{Asp145}] - [H_{Asp145}\cdots N_{Cys126}] + [N_{Cys126}\cdots H_{Cys126}] - [H_{Cys126}\cdots S_{Cys126}]$, is given in Å. (B) Evolution of the PMF for the modeled reaction as a function of the simulation time set for each US window. (C) Comparison between the PMF for the forward reaction (run #1) and the backward reaction (run #2), obtained from US windows of 350 ps each. (D) Single-point energy calculations in the gas phase for model systems composed of an N-terminal cysteine and acetic acid.

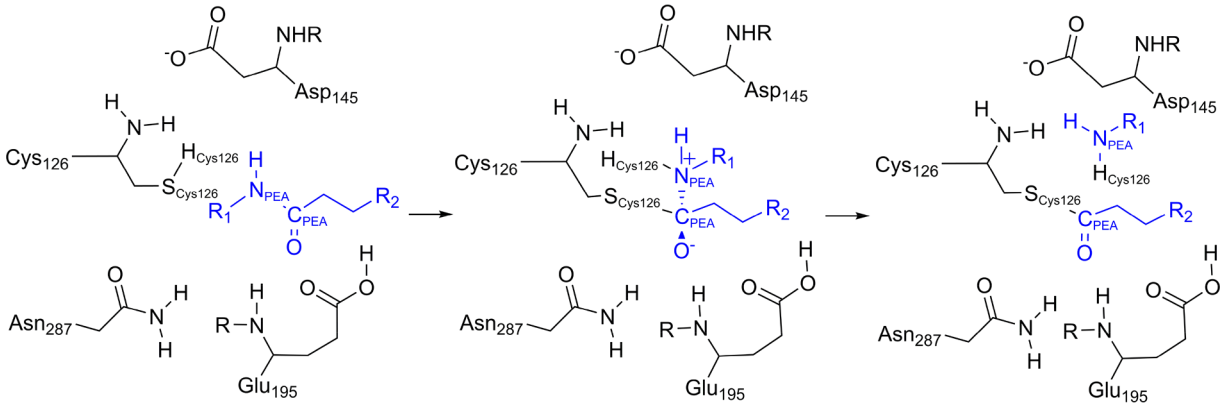

Figure 6. Postulated mechanism of NAAA acylation (mechanism ***m1***) occurring through protonation of PEA at the nitrogen atom by the Cys126 thiol group, simulated by QM/MM using adiabatic mapping and US. The ethanol chain at the nitrogen atom of PEA (R_1) and the complete chain of the palmitic acid moiety of PEA (R_2) are not displayed.

indicates that differences among free-energy minima converge after 250 ps of QM/MM US per window (Figure 5B). We also established that the simulated process is reversible: i.e., that configuration **#3** can readily convert into **#4** with a similar PMF (Figure 5C). Finally, we evaluated the ability of the DFTB3 semiempirical method to give reasonable reaction energies for the proton transfer reactions investigated here. Starting from the optimized geometries of the NAAA-PEA complex, we built a set of molecular models composed of cysteine and acetic acid in three different protonation states

https://dx.doi.org/10.1021/acscatal.0c02903
ACS Catal. 2020, 10, 11797−11813

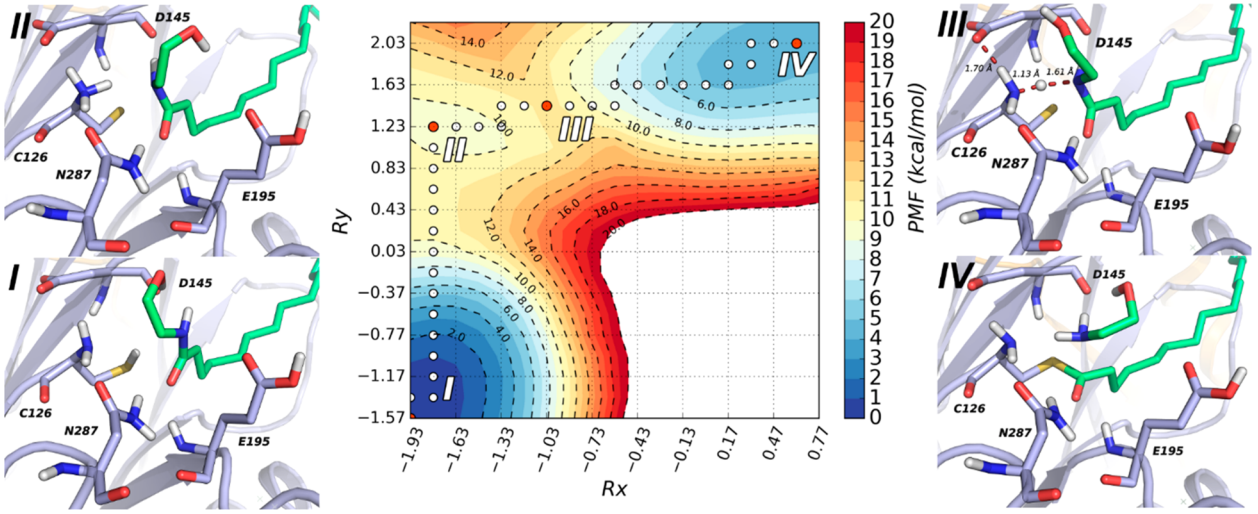

Figure 7. FES for NAAA acylation calculated at the DFTB3/AMBER level for mechanism ***m1***. Free energy values are given in kcal mol^{-1}, while reaction coordinates Rx and Ry are given in Å. White and red dots on the FES represent the 36 US windows corresponding to the minimum free-energy path connecting reactants (*I*) to products (*IV*). Relevant configurations on the minimum free-energy path are displayed. Definitions: (*I*) Michaelis complex (corresponding to the 1st window, with Rx and Ry equal to −1.93 and −1.57 Å, respectively); (*II*) zwitterionic Cys126 with the deplanarized amide of PEA (corresponding to the 16th window, with Rx and Ry equal to −1.78 and 1.23 Å, respectively); (*III*) transition state (TS, corresponding to the 22nd window, with Rx and Ry equal to −1.03 and 1.43 Å, respectively); (*IV*) acylated NAAA with expelled ethanolamine (corresponding to the 36th window, with Rx and Ry equal to 0.62 and 2.03 Å, respectively). NAAA is represented with violet carbon atoms and PEA with green carbon atoms.

corresponding to configurations **#3**−**#5**. Single-point energy calculations were performed at different levels of theory (see the Supporting Information for details). Figure 5D shows that B3LYP-D3 and MP2 give potential energy values in reasonable agreement with DFTB3, suggesting that this method has acceptable accuracy under the present conditions.

Catalytic Mechanism for NAAA Acylation. Having identified configuration **#3** (Figure 2) as the most relevant protonation state in NAAA, we turned to consider the mechanism for NAAA acylation. We hypothesized a reaction path in which Cys126 initiates catalysis through protonation of the amide nitrogen of PEA, similarly to what had been reported for other cysteine amidases,[39] including Ntn-hydrolases[40] and papain-like cysteine proteases.[41,42] A reaction mechanism was modeled in which the protonation of PEA nitrogen is accompanied by a nucleophilic attack to form a zwitterionic tetrahedral intermediate (TI), which eventually evolves toward the formation of the acylenzyme with concurrent expulsion of ethanolamine (mechanism ***m1***, Figure 6).

A frame taken from a QM/MM MD trajectory of the NAAA-PEA complex was transformed into the acylenzyme by restraining the system along two RCs, named Rx and Ry, by adiabatic mapping. Rx was defined as the difference between the nucleophilic attack distance (S_{Cys126}, C_{PEA}) and the leaving group expulsion distance (N_{PEA}, C_{PEA}), while Ry was described by the difference between the distance separating the nucleophilic sulfur from its acid proton (S_{Cys126}, H_{Cys126}) and the distance separating the same proton from PEA nitrogen (H_{Cys126}, N_{PEA}). The resulting potential energy surface (PES) for acylation is reported in Figure S10 in the Supporting Information. The configurations generated by adiabatic mapping were used for running US simulations. This allowed us to estimate the change in free energy associated with the progress of the reaction.

The free energy surface (FES) illustrated in Figure 7 shows that acylation is a highly concerted process. The FES of NAAA acylation indicates that the TI is not a minimum but a transient configuration along the reaction pathway. The FES shows the presence of a sharp transition state (TS) area, featuring a free energy of 11−12 kcal mol^{-1} above the level of the reactants, and two other minima in addition to the Michaelis complex. The first minimum, located close to the top left corner of the surface, describes structures in which the proton of the Cys126 thiol has been transferred to the N-terminal amine of the same cysteine, generating a positive charge on the basic nitrogen, which is stabilized by the carboxylate group of Asp145 (structure *II*, Figure 7). The second minimum, placed in the top right corner of the FES, describes geometries corresponding to the acylenzyme (structure *IV*, Figure 7), with a novel S−C bond being formed, the carbonyl oxygen of the thioester adduct forming two H-bonds with the oxyanion hole, and the ethanolamine leaving group interacting with the Asp145 backbone oxygen.

Analysis of the US trajectories along the minimum free energy path, identified within a grid of 19 × 20 points (along Rx and Ry, respectively) by an iterative procedure (see Methods and section 10 in the Supporting Information), allows us to propose the following mechanism for NAAA acylation. The first relevant event is represented by deplanarization of the amide of PEA, which occurs as the thiol group approaches the scissile C−N bond. This event, which is favored by the presence of an H-bond between the NH group of PEA and the carbonyl backbone oxygen of Asp145, increases the basicity of the PEA nitrogen, thus lowering the energetic cost of its subsequent protonation by Cys126.[43,44] As anticipated earlier, the thiol proton of Cys126 is not directly transferred to the PEA nitrogen. Instead, this hydrogen first forms a covalent bond with the N-terminal amine group of the same cysteine, generating a zwitterionic Cys126. The reaction proceeds by passing through the main

https://dx.doi.org/10.1021/acscatal.0c02903
ACS Catal. 2020, 10, 11797−11813

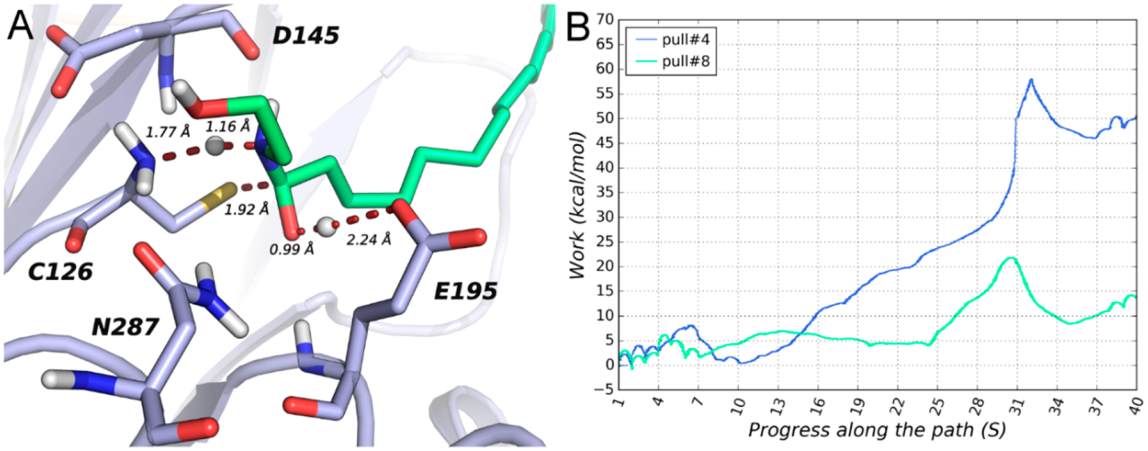

Figure 8. Mechanism of NAAA acylation involving Glu195 as acid. (A) Model of the cationic TI, where NAAA is represented with violet carbon atoms and PEA with green carbon atoms. Distances between key atoms involved in the reaction are given in Å. (B) Work curves projected along *S* for steered-MD simulations. pull #4 is an early run of the optimization procedure of the reaction path by PCV, and pull #8 is the final run and describes the energetics of the optimized path.

TS in which the Cys126 transfers the former thiol proton to the PEA nitrogen (structure *III*, Figure 7). Visual inspection of the TS structure shows that in this configuration the Cys126 sulfur and PEA carbonyl carbon have not formed a new covalent bond yet, as their mutual distance is around 2.2 Å (Figure S11 in the Supporting Information), substantially higher than the 1.8 Å value found in the acylenzyme. The reaction thus proceeds with the progressive reduction in the C−S distance and a simultaneous increase in the C−N distance of PEA, eventually leading to the formation of the acylenzyme with expulsion of the ethanolamine. This process is convoyed by a significant drop in the free energy of the system, as indicated by the flat area occupied by state *IV* on the FES reported in Figure 7.

A replica of this simulation, started from a different frame of the QM/MM MD trajectory, gives an almost identical FES (see Figure S12 in the Supporting Information) with an energetic barrier of 11−12 kcal mol^{-1}.

The mechanism represented in Figure 7 thus emerges as a consistent pathway for NAAA acylation. Mutation of N292A[8] in rat NAAA (corresponding to hNAAA N287A) causes a marked reduction in catalytic activity, confirming the importance of the asparagine side chain for the oxyanion hole. In line with mutagenesis data reporting the loss of hydrolytic activity for three mutant variants of Asp145,[8,18,21] in our simulation the carboxylate group of Asp145 emerges as a critical factor in the stabilization of intermediate *II* and of the main TS of acylation. Nonetheless, we tested if Asp145 modeled in its neutral form (i.e., proton configuration **#2** in Figure 2) might give a better free energy profile. The analysis of the FES reveals that the free energy for acylation is higher, with the proton transfer from the thiol group of Cys126 to the N-terminal amine characterized by a barrier of 15−16 kcal mol^{-1} (Figure S13 in the Supporting Information), due to the loss of the stabilizing effect of the negative charge of the Asp145 side chain on the positively charged intermediate.

Alternative Paths for NAAA Acylation. We next asked whether alternative pathways of NAAA acylation could provide better reaction energetics in comparison to the proposed mechanism ***m1***. We hypothesized that acylation of Cys126 may be favored by the protonation of the carbonyl oxygen of PEA by the thiol group (mechanism ***m2***, Figure S14 in the Supporting Information). This mechanism involves the formation of a neutral TI, upon protonation of the carbonyl oxygen of PEA by the thiol and nucleophilic attack by the thiolate. Calculations show that the neutral TI is a high-energy state (Figure S15A in the Supporting Information) prone to spontaneous transformation in the Michaelis complex (Figure S15B in the Supporting Information). An acylation process based on the formation of this TI is thus unlikely.

Another conceivable pathway might involve Glu195, which being modeled in neutral form to stabilize the active site of NAAA could donate its proton to the PEA carbonyl oxygen (mechanism ***m3***, Figure S16 in the Supporting Information). The protonated PEA could then react with Cys126, with the thiol group protonating the nitrogen of ethanolamine, via the N-terminal group of the cysteine, and the thiolate attacking the carbonyl carbon. The final step of this reaction would see the acylenzyme donating the proton back to the carboxylate group of Glu195. The simulation of this mechanism is complicated by the lack of stable intermediates, which prevents the possibility of separating Cys126 acylation into distinct chemical steps. To overcome this issue, we modeled this reaction with a path-collective variable (PCV) method.[24] This approach allows us to explore a mechanism with only two variables, one (*S*) describing the progress along the path and the other (*Z*) defining the distance from the path (see the Supporting Information for details). At first, we verified the ability of the QM/MM PCV approach to reproduce the sequence and the relative energetic penalties of NAAA acylation obtained by US in the case of mechanism ***m1*** (Figures S17 and S18 in the Supporting Information). As the PCV approach well approximated the minimum-energy path of US simulations at lower computational cost (approximately one-fourth, see section 16 in the Supporting Information), we modeled mechanism ***m3*** in the *S*/*Z* space at the DFTB3/AMBER level.

An initial guess-path was generated by building geometries corresponding to the configurations reported in Figure S16. Then an optimization of the reaction path was performed by QM/MM steered-MD simulations. During the first run, protonation of the carbonyl oxygen of PEA by Glu195 and nucleophilic attack by the thiolate gives a neutral TI, which is further protonated at the amide nitrogen by the Cys126

https://dx.doi.org/10.1021/acscatal.0c02903
ACS Catal. 2020, 10, 11797−11813

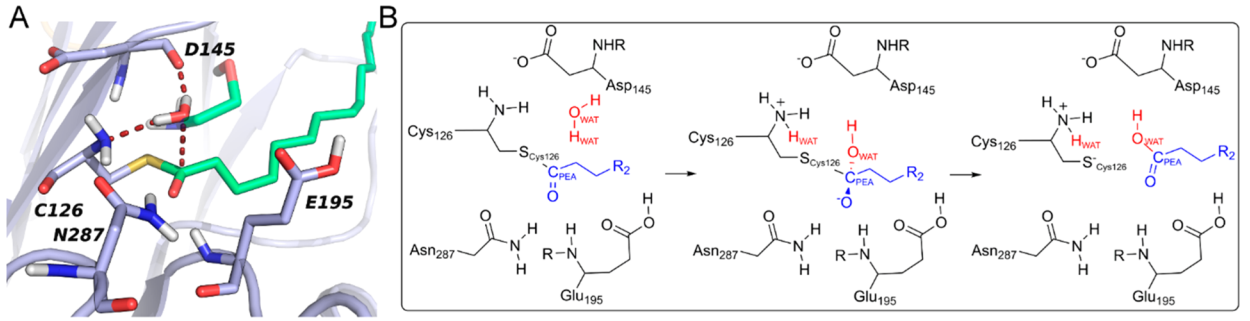

Figure 9. (A) NAAA in its acylated form. The deacylating water molecule is displayed together with its H-bonds with the active site. The ethanolamine molecule expelled at the end of the acylation step is shown superposed on the water molecule. (B) Postulated mechanism for NAAA deacylation simulated by QM/MM using adiabatic mapping and umbrella sampling. R_2 indicates a palmitic acid chain.

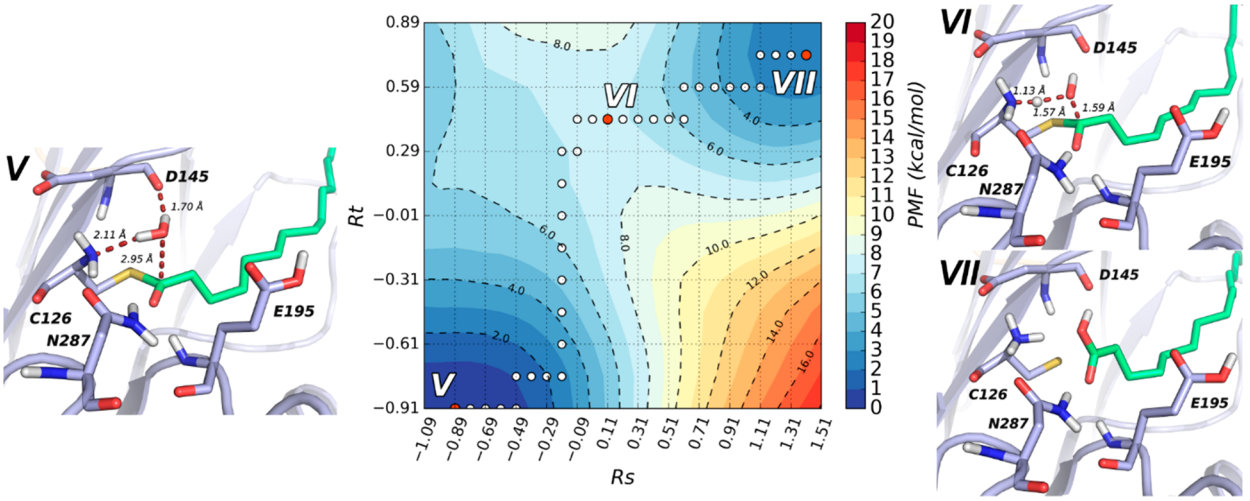

Figure 10. FES for NAAA deacylation calculated at the DFTB3/AMBER level. Free energy values are given in kcal mol^{-1}, and reaction coordinate Rs and Rt are expressed in Å. White and red dots on the FES represent the 35 US windows corresponding to the minimum free energy path connecting reactants (*V*) to products (*VII*). Relevant configurations on the minimum free-energy path are displayed. Definitions: (*V*) acylenzyme and the deacylating water molecule (corresponding to the 1st window, with Rs and Rt equal to −0.89 Å and −0.91 Å, respectively); (*VI*) transition state (TS, corresponding to the 11th window, with Rs and Rt equal to 0.11 and 0.44 Å, respectively); (*VII*) palmitic acid and free enzyme (corresponding to the 35th window, with Rs and Rt equal to 1.41 and 0.74 Å, respectively). NAAA is represented with violet carbon atoms and palmitic acid with green carbon atoms.

ammonium group, resulting in a cationic TI (Figure 8A) and then evolves to the acylenzyme product. However, subsequent steered-MD simulations change the reaction mechanism and the optimized path becomes similar to that of Figure 7 (Figure S19 in the Supporting Information). The barrier for NAAA acylation passes from 60 kcal mol^{-1} of an early run (pull #4) to 22 kcal mol^{-1} of the last run (pull #8), where Glu195 does not participate in catalysis (Figure 8B).

Catalytic Mechanism for NAAA Deacylation. The acylenzyme resulting from the transfer of a palmitoyl group to the sulfur of Cys126 (configuration *IV* in Figure 7) was used to generate a starting point for modeling the deacylation step. The ethanolamine group was removed from the active site (see Methods), and the resulting system was equilibrated by QM/MM MD. During this simulation a water molecule undertakes a number of hydrogen bonds with the NAAA active site, occupying a position similar to that of the amine group of ethanolamine at the end of the acylation step (Figure 9A). The distance separating the oxygen of this water and the carbonyl carbon of the thioester is frequently lower than 3.0 Å, while the angle between the water oxygen and the carbonyl is close to 90°, approaching the ideal value for a nucleophilic attack. Similarly to what was done in the study of FAAH deacylation,[45] this water molecule was selected as the deacylating molecule. We postulated that deacylation occurs with no change in the proton distribution of the active site residues. Accordingly, the N-terminal amino group of Cys126 acts as a base to increase the nucleophilicity of the water molecule (Figure 9B). The subsequent attack at the thioester carbon leads to a TI, which decomposes, giving zwitterionic Cys126 and palmitic acid. Once this reaction is completed, Cys126 can equilibrate with its preferred neutral protonation state by an internal proton transfer, to start another catalytic cycle.

To simulate Cys126 deacylation, we transformed the acylenzyme into palmitic acid and free zwitterionic NAAA by progressively restraining the system along two reaction coordinates, named Rs and Rt, using the adiabatic mapping approach. Rs is defined as the difference between the nucleophilic attack distance (O_{WAT}, C_{PEA}) and the leaving group expulsion distance (S_{Cys126}, C_{PEA}), while Rt is the difference between the distance separating the water oxygen from its proton (O_{WAT}, H_{WAT}) and the distance separating the same proton from the nitrogen of Cys126 (H_{WAT}, N_{Cys126}).

https://dx.doi.org/10.1021/acscatal.0c02903
ACS Catal. 2020, 10, 11797−11813

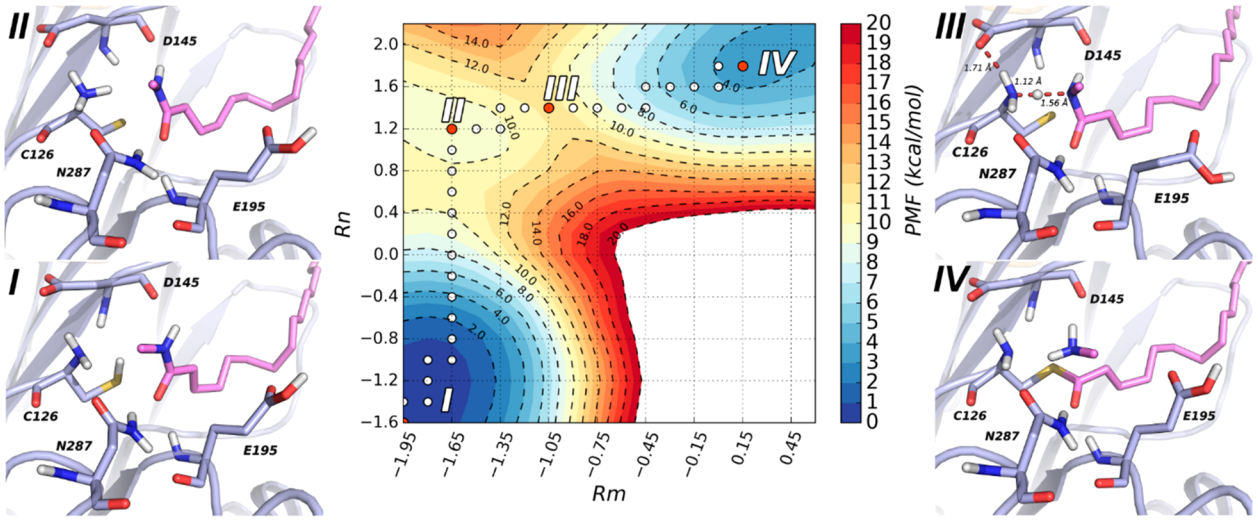

Figure 11. FES for NAAA acylation by PMA calculated at the DFTB3/AMBER level. Potential energy and free energy are given in kcal mol^{-1}, and the reaction coordinates Rm and Rn are expressed in Å. White and red dots on the FES represent the 32 US windows corresponding to the minimum free energy path connecting reactants (*I*) and products (*IV*). Key configurations on the minimum free energy path are displayed. Defintions: (*I*) Michaelis complex (corresponding to the 1st window with Rm and Rn equal to −1.95 and −1.60 Å, respectively); (*II*) zwitterionic Cys126 with deplanarized amide (corresponding to the 17th window, with Rm and Rn equal to −1.65 and 1.20 Å, respectively); (*III*) transition state (TS, corresponding to the 22nd window, with Rm and Rn equal to −1.05 and 1.40 Å, respectively); (*IV*) acylated NAAA with methylamine (corresponding to the 32nd window, with Rm and Rn equal to 0.15 and 1.80 Å, respectively). NAAA is represented with violet carbon atoms and PMA with pink carbon atoms.

The resulting PES is reported in Figure S20 in the Supporting Information. The configurations generated by adiabatic mapping were used to run US simulations along the reaction coordinates Rs and Rt, which allowed us to retrieve the corresponding FES (Figure 10). An analysis of this surface shows that deacylation is a concerted process, where the TI is a transient configuration and not a free energy minimum. The area of the TS is characterized by geometries in which the water proton has been transferred to the amino group of Cys126, while the nucleophilic attack is still occurring (Figure 10, state *VI*). Conclusion of the nucleophilic attack triggers the expulsion of the thiolate group of Cys126, leading to the formation of free NAAA and palmitic acid (Figure 10, state *VII*). The free energy barrier for deacylation is 7 kcal mol^{-1}, indicating that the hydrolysis of PEA is controlled by the acylation step.

Role of the Ethanolamine Head during Acylation. To probe if the ethanolamine head has a role during acylation, the geometries assumed by this fragment within the US windows of the minimum free energy path connecting the Michaelis complex (*I*) to the acylenzyme (*IV*) of Figure 7 were analyzed. Along the path, the hydroxyl group of PEA engages in different transient polar interactions with the active site of NAAA. In the Michaelis complex, and during the early phase of acylation, the hydroxyl group forms hydrogen bonds with the backbone carbonyl of Asp145 for half of the simulation and with the solvent or with the CO of the Asn287 side chain for the rest (Figure S21 in the Supporting Information). As the reaction proceeds along the path, the hydroxyl group of PEA does not exhibit a preference for a specific NAAA residue, but it alternatively interacts with the carbonyl fragment of the Glu195 side chain, the backbone carbonyl of Asp145, or a water molecule (Figure S21 in the Supporting Information). As this behavior does not propose a specific role for the PEA head, we simulated the mechanism of NAAA acylation for palmitoyl methyl amide (PMA), a secondary fatty acid amide that lacks the terminal hydroxyl (PES reported in Figure S22 in the Supporting Information). The resulting FES indicates that also for PMA acylation is a concerted process (Figure 11). The TS area is characterized by geometries in which a proton is being transferred to the methylamine leaving group (Figure 11, structure *III*). Protonation triggers the breakage of the C−N bond with the formation of acylated NAAA and free methylamine (Figure 11, structure *IV*). The activation barrier deduced from the FES corresponds to 11−12 kcal mol^{-1}, close to that found for PEA.

We determined the kinetics of PEA and PMA hydrolysis by rat NAAA using a liquid chromatography/mass spectrometry (LC/MS) assay (see Methods). A Michaelis−Menten analysis (Figure 12) shows that the substrates display comparable K_m values (19.8 μM for PEA; 18.1 μM for PMA) but different

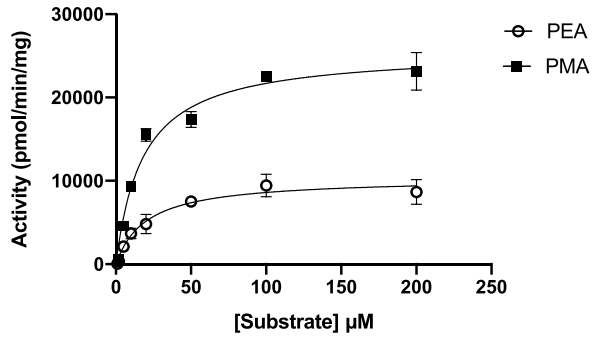

Figure 12. Michaelis−Menten analysis of PEA (empty circles) and PMA (filled squares) hydrolysis by rat NAAA. The activity is expressed as picomoles of product (palmitate) produced per minute per milligram of protein in the lysosomal extract. The results are shown as mean ± SEM (each measure was conducted in triplicate). Confidence limits at the 95% level for fitted parameters: PEA, K_m 13.3−29.4 μM, V_{max} 9.1 × 10^3 to 11.6 × 10^3 pmol min^{-1} mg^{-1}; PMC, K_m 13.9−23.5 μM, V_{max} 23.7 × 10^3 to 27.7 × 10^3 pmol min^{-1} mg^{-1}.

https://dx.doi.org/10.1021/acscatal.0c02903
ACS Catal. 2020, 10, 11797−11813

reaction rates under saturating conditions. The V_{max} parameter obtained for PMA (25.6×10^3 pmol min^{-1} mg^{-1}) is even higher than that of PEA (10.3×10^3 pmol min^{-1} mg^{-1}). Indeed, supporting the conclusion that the hydroxyl group of PEA may be dispensable for catalysis, the catalytic efficiency is higher when the more lipophilic PMA is used as the substrate.

DISCUSSION

The crystal structures of NAAA revealed several important aspects related to how this enzyme recognizes and cleaves PEA, but they also raised important questions regarding the catalytic mechanism. First, the proton configuration of the ionizable groups surrounding the catalytic site is expected to affect not only the electrostatics of this region but also the stability of structural domains of NAAA that scaffold the N-terminal nucleophile Cys126. Given the optimal activity of NAAA at pH 4−5,[20] it is likely that some carboxylate groups of aspartic and glutamic residues are neutral, while others are in an anionic state. While a fast proton-exchange equilibrium with water is expected for solvent-exposed residues, specific protonation states for amino acids surrounding the catalytic site are critical for MD simulations. Second, the protonation state of residues directly involved in PEA hydrolysis (Cys126 and Asp145 for hNAAA) and the atomistic details of the catalytic mechanism cannot be definitely inferred from X-ray structures.

Using MD simulations with two different force fields, we evaluated the structural stability of NAAA models with different protonation states for several carboxylic side chains and for the N-terminal Cys126. These simulations showed that the architecture of the catalytic site is stabilized by protonation of most of the aspartic and glutamic residues surrounding Cys126 and Arg300. This is consistent with the marked decrease in activity at neutral pH, where most carboxylic groups are expected to be deprotonated. The only protonic configurations that preserved the active site geometry of a crystallized complex of NAAA with its noncovalent inhibitor ARN19702 presented a neutral N-terminal amine with either a neutral thiol and an anionic carboxylate on the side chain of Asp145 (system **#3** in Figure 2) or a thiolate anion and a neutral Asp145-carboxylic acid (system **#4** in Figure 2). As the catalytic process takes place at pH 4−5, a neutral amine is unexpected. On the other hand, the electrostatic environment of Cys126, with the guanidinium group of Arg300 placed at an H-bond distance from the N-terminal amine of the cysteine in different crystal structures (e.g., 3.02 Å in 6DXX, chains C and D, between the nitrogen atoms) can strongly disfavor the protonation of this group. The importance of Arg300 for Ntn-hydrolases working at acidic pH is highlighted by the nearly complete suppression of amidase activity for the corresponding R333Q mutation in acid ceramidase.[21]

The three ionizable groups of Cys126 and Asp145 are involved in a prototropic equilibrium. We investigated this equilibrium by US at the QM/MM level. The resulting PMF indicates that the preferred state for Cys126 is neutral ($-NH_2$/$-SH$), even if the thiol proton can be easily transferred to the amino group to generate a zwitterion thanks to the stabilization of the ammonium provided by the carboxylate group of Asp145.

Starting from the minimum-energy state with neutral Cys126, the mechanism of PEA hydrolysis catalyzed by NAAA was investigated through extensive QM/MM calculations. Acylation was the rate-limiting step, with a free energy barrier of 11−12 kcal mol^{-1}. Similarly to what has been reported for FAAH,[46] the other hydrolase contributing to PEA catabolism in vivo, QM/MM simulations propose a catalytic mechanism in which leaving-group protonation emerges as the critical step of acylation. During acylation, NAAA's N-terminal cysteine acts both as an acid, protonating the amide nitrogen of PEA, and as a nucleophile, promoting the breakage of the C−N bond of PEA. The reaction is concerted and involves the generation of a transient state in which Cys126 is present in a zwitterionic form. The formation of this state is accompanied by deplanarization of the amide of PEA, which is a critical step for amide hydrolysis, as it increases the basicity of the amide nitrogen[47,48] and favors its subsequent protonation by Cys126. The carboxylate group of Asp145 helps proton transfer from Cys126 to the substrate, but it does not directly participate in the reaction. The presence of a single residue acting as a catalytic center emerges as a distinguishing feature of NAAA, in comparison to classical Ser-His-Asp hydrolases and other unconventional amidases, including FAAH.[49] Alternative mechanisms of NAAA acylation, based on the protonation of the amide oxygen of PEA by Cys126 or by Glu195, were also explored, but they were characterized by less favorable reaction energetics. Reaction barriers calculated using the DFTB3/3OB semiempirical method could be underestimated.[50,51] On the other hand, the DFTB3 method has been recently used to describe reaction mechanisms in β-lactamases[52] and in cysteine proteases,[53] providing reaction energetics in qualitative agreement with calculations performed at the MP2 level. This suggests that DFTB3 can be used to compare alternative reaction mechanisms with fair confidence.

Deacylation is a fast process, with a barrier of 7 kcal mol^{-1}. During this reaction, the N-terminal amino group of Cys126 activates the deacylating water molecule while the thioester carbonyl interacts with the oxyanion hole. This favorable free energy profile suggests that acylenzyme hydrolysis requires a specific arrangement of the thioester group and of the nucleophilic water to occur. It is known that NAAA is inhibited by lactone[8,54] and lactam derivatives,[55] which acylate the catalytic cysteine,[56] yielding thioesters resistant to hydrolysis. Crystal structures of NAAA acylated by a lactam inhibitor[19] show that the thioester carbonyl is out of the oxyanion hole, which is instead occupied by an amide-like group (i.e., a carbamate) in the recognition portion of the inhibitor. Our results provide an explanation for the importance of the recognition group that occupies the oxyanion hole, which was previously highlighted by structure−activity relationship studies.[54,55]

We also evaluated a possible catalytic role for Glu195, as this residue contributes to the pH−activity profile of hNAAA. Ueda and collaborators had shown that this residue is responsible for the high activity of NAAA at pH 4.5. Its mutation to glutamine (E195Q) or alanine (E195A) reduces the hydrolytic activity of NAAA by 4- and 10-fold, respectively, and flattens the activity peak in the pH interval from 4 to 5.[20] The observation that its neutral form is required for the stability of the active site model in MD simulations (Figure 3 and Figures S5 and S6) is consistent with a maximum activity at pH 4−5. While a direct involvement of the carboxyl group of Glu195 at the beginning of the catalytic cycle has been ruled out by QM/MM simulations, it is also possible that this group assists the reaction in a different way. At the end of the acylation step, the free energy of the acylenzyme−ethanolamine complex is 5 kcal/mol higher than that of the Michaelis

https://dx.doi.org/10.1021/acscatal.0c02903
ACS Catal. 2020, 10, 11797−11813

complex, which makes aminolysis of the acylenzyme a possible event. At low pH values the protonation of ethanolamine may occur spontaneously, thus preventing the backward reaction, but it is worth noting that, at the end of acylation, Glu195 is the only acid residue within 5 Å of the ethanolamine nitrogen. Its carboxylic group could protonate the amine of the product, thus favoring its removal from the active site and promoting the entrance of a deacylating water molecule.

Prior theoretical investigations on the catalytic mechanism of Ntn-hydrolases in the presence of substrates include penicillin acylase (PA),[57] aspartylglucosaminidase (AGA),[58] γ-glutamyl transpeptidase (GGT),[59] and conjugated bile acid hydrolase (CBAH).[40] PA is a serine hydrolase, and AGA and GGT are threonine hydrolases, while CBAH is a cysteine hydrolase belonging to the same enzyme superfamily of NAAA.[1] All of the mechanisms previously modeled propose a nucleophilic attack of the side chain to the substrate carbonyl, favored by the nucleophile deprotonation, and a proton transfer from the terminal amine group to the amide nitrogen of the substrate. On comparison of our finding to what was previously reported for CBAH, a fundamental difference is with regard to the dominant protonation state of the N-terminal cysteine in the Michaelis complex. In the case of NAAA, the neutral form of Cys126 was more stable than the zwitterionic form, while for CBAH the zwitterionic form emerged as the most stable state. The difference in the calculated free energy for these protonation states in NAAA and CBAH could be due not only to the different DFTB methods employed (SCC-DFTB[32] for CBAH and DFTB3[30] for NAAA) but also to a different consideration of the conformational flexibility of active site residues. In the case of NAAA, MD simulations reveal that protonation states of specific carboxylate groups heavily affect the interaction of the guanidine group of Arg300 with the N-terminal amine of Cys126. Not only this interaction is critical to guarantee the overall stability of the catalytic machinery but also it modulates the amine basicity by avoiding overprotonation of the catalytic cysteine. In this regard, Gebai et al.[21] suggested for acid ceramidase, a close NAAA homologue with optimal activity at acidic pH, a mechanism starting from a cationic (ammonium) form of the N-terminal cysteine Cys143 (Cys126 in hNAAA), with a proton shift from the ammonium group to the carboxylate of the critical Asp162 (Asp145 in hNAAA). The corresponding state in NAAA has one more proton on the catalytic "dyad" Cys126-Asp145 in comparison to that in our starting configuration. While at the low pH values needed for NAAA and AC activity this overprotonated state appears possible, when we modeled NAAA acylation with protonated Asp145 and neutral Cys126, the reaction path had a significantly higher free energy barrier.

Finally, our study also provides information about structure−activity relationships for PEA derivatives that can be NAAA substrates. The mobility of the terminal hydroxyl in the ethanolamine head suggests that this group could be less important for PEA hydrolysis by NAAA than for its biological effects. By modeling the acylation step for PMA, we obtained a very similar FES, which indicates a negligible role of this group in the rate-limiting step of the catalysis. Accordingly, PMA is hydrolyzed by rat NAAA, which has 79% identity with hNAAA, with a catalytic efficiency similar to that for PEA. Our findings thus suggest that the substrate selectivity of NAAA is predominantly governed by the stereoelectronic properties of the fatty acyl chain of the substrate.

CONCLUSIONS

We used a multiscale computational approach based on classical MD and a QM/MM approach linked to enhanced sampling methods to elucidate the catalytic mechanism of the Ntn-cysteine amidase NAAA. The results of our simulations show that the protonation state of NAAA is critical for catalysis and that the key residue Cys126 acts both as a nucleophile and as an acid in distinct steps of the catalytic process. Acylation is the rate-limiting event of the entire hydrolysis process, with leaving group protonation emerging as the critical step of the entire catalytic cycle. Simulations and kinetic experiments indicate that the terminal hydroxyl group of PEA plays little or no role in catalysis. Our findings will be useful to assist the design of selective NAAA substrates and of novel covalent inhibitors targeting Cys126.

ASSOCIATED CONTENT

Supporting Information

The Supporting Information is available free of charge at https://pubs.acs.org/doi/10.1021/acscatal.0c02903.

Detailed analysis of MD simulations performed with OPLS3 and AMBER, computational results for alternative mechanisms for acylation by US or PCV simulations, technical details regarding the preparation of the NAAA-PMA complex and relative QM/MM US simulations at the DFTB3/AMBER level, and the synthetic procedure for the chemical synthesis of PEA and PMA substrates, including compound characterization and purity (PDF)

Geometries of key states (*II*−*VII*) along the minimum free-energy path for acylation and deacylation starting from the NAAA-PEA Michaelis complex (ZIP)

AUTHOR INFORMATION

Corresponding Authors

Alessio Lodola − *Dipartimento di Scienze degli Alimenti e del Farmaco, Università degli Studi di Parma, I-43124 Parma, Italy;* orcid.org/0000-0002-8675-1002; Phone: +39 0521 905062; Email: alessio.lodola@unipr.it; Fax: +39 0521 905006

Marco Mor − *Dipartimento di Scienze degli Alimenti e del Farmaco, Università degli Studi di Parma, I-43124 Parma, Italy;* orcid.org/0000-0003-0199-1849; Phone: +39 0521 905059; Email: marco.mor@unipr.it; Fax: +39 0521 905006

Authors

Laura Scalvini − *Dipartimento di Scienze degli Alimenti e del Farmaco, Università degli Studi di Parma, I-43124 Parma, Italy;* orcid.org/0000-0003-3610-527X

Andrea Ghidini − *Dipartimento di Scienze degli Alimenti e del Farmaco, Università degli Studi di Parma, I-43124 Parma, Italy;* orcid.org/0000-0003-1575-975X

Donatella Callegari − *Dipartimento di Scienze degli Alimenti e del Farmaco, Università degli Studi di Parma, I-43124 Parma, Italy;* orcid.org/0000-0002-2574-3826

Silvia Rivara − *Dipartimento di Scienze degli Alimenti e del Farmaco, Università degli Studi di Parma, I-43124 Parma, Italy;* orcid.org/0000-0001-8058-4250

Daniele Piomelli − *Department of Anatomy and Neurobiology, Department of Pharmaceutical Sciences, and Department of Biological Chemistry and Molecular Biology, University of*

California, Irvine, California 92697-4625, United States; orcid.org/0000-0002-2983-774X

Complete contact information is available at: https://pubs.acs.org/10.1021/acscatal.0c02903

Author Contributions

The manuscript was written through contributions of all authors. All authors have given approval to the final version of the manuscript.

Funding

This work was partially supported by the Italian Ministry for University and Research (MIUR, PRIN 2017, 20175SA5JJ project, to M.M.) and the University of Parma (Progetti di Ateneo FIL Quota Incentivante 2019, to A.L. and S.R.). This research benefitted from the HPC (High Performance Computing) facility of the University of Parma, Italy (http://www.hpc.unipr.it) and the support of CINECA (ISCRA project NAAAQM-HP10CDBFBQ, to L.S.).

Notes

The authors declare the following competing financial interest(s): the following authors are inventors of patents and patent applications (owned by University of California, University of Urbino, and University of Parma) that protect composition of matter and use of various NAAA inhibitor classes: D.P., WO 2009049238, WO 2013078430, WO 2014144547, WO 2014144836; M.M., WO 2009049238, WO 2013078430, WO 2014144547, WO 2014144836.

■ ACKNOWLEDGMENTS

Support from the *Teach in Parma* project and the Fondazione Cariparma (to D.P. and A.G.) is kindly acknowledged. Dr. Bhushan Nagar is kindly acknowledged for providing the hNAAA structure in advance and for a critical reading of the manuscript.

■ REFERENCES

(1) Tsuboi, K.; Sun, Y. X.; Okamoto, Y.; Araki, N.; Tonai, T.; Ueda, N. Molecular characterization of N-acylethanolamine-hydrolyzing acid amidase, a novel member of the choloylglycine hydrolase family with structural and functional similarity to acid ceramidase. *J. Biol. Chem.* **2005**, *280*, 11082−11092.

(2) Désarnaud, F.; Cadas, H.; Piomelli, D. Anandamide amidohydrolase activity in rat brain microsomes. Identification and partial characterization. *J. Biol. Chem.* **1995**, *270*, 6030−6035.

(3) Ueda, N.; Tsuboi, K.; Uyama, T. N-acylethanolamine metabolism with special reference to N-acylethanolamine-hydrolyzing acid amidase (NAAA). *Prog. Lipid Res.* **2010**, *49*, 299−315.

(4) Devane, W. A.; Hanus, L.; Breuer, A.; Pertwee, R. G.; Stevenson, L. A.; Griffin, G.; Gibson, D.; Mandelbaum, A.; Etinger, A.; Mechoulam, R. Isolation and structure of a brain constituent that binds to the cannabinoid receptor. *Science* **1992**, *258*, 1946−1949.

(5) Kuehl, F. A., Jr.; Jacob, T. A.; Ganley, O. H.; Ormond, R. E.; Meisinger, M. A. P. The identification of N-(2-hydroxyethyl)-palmitamide as a naturally occurring anti-inflammatory agent. *J. Am. Chem. Soc.* **1957**, *79*, 5577−5578.

(6) Lo Verme, J.; Fu, J.; Astarita, G.; La Rana, G.; Russo, R.; Calignano, A.; Piomelli, D. The nuclear receptor peroxisome proliferator-activated receptor-alpha mediates the anti-inflammatory actions of palmitoylethanolamide. *Mol. Pharmacol.* **2005**, *67*, 15−19.

(7) Lo Verme, J.; Russo, R.; La Rana, G.; Fu, J.; Farthing, J.; Mattace-Raso, G.; Meli, R.; Hohmann, A.; Calignano, A.; Piomelli, D. Rapid broad-spectrum analgesia through activation of peroxisome proliferator-activated receptor-alpha. *J. Pharmacol. Exp. Ther.* **2006**, *319*, 1051−1061.

(8) Solorzano, C.; Zhu, C.; Battista, N.; Astarita, G.; Lodola, A.; Rivara, S.; Mor, M.; Russo, R.; Maccarrone, M.; Antonietti, F.; Duranti, A.; Tontini, A.; Cuzzocrea, S.; Tarzia, G.; Piomelli, D. Selective N-acylethanolamine-hydrolyzing acid amidase inhibition reveals a key role for endogenous palmitoylethanolamide in inflammation. *Proc. Natl. Acad. Sci. U. S. A.* **2009**, *106*, 20966−20971.

(9) Bottemanne, P.; Muccioli, G. G.; Alhouayek, M. N-acylethanolamine hydrolyzing acid amidase inhibition: tools and potential therapeutic opportunities. *Drug Discovery Today* **2018**, *23*, 1520−1529.

(10) Tuo, W.; Leleu-Chavain, N.; Spencer, J.; Sansook, S.; Millet, R.; Chavatte, P. Therapeutic potential of fatty acid amide hydrolase, monoacylglycerol lipase, and N-acylethanolamine acid amidase inhibitors. *J. Med. Chem.* **2017**, *60*, 4−46.

(11) Tsuboi, K.; Takezaki, N.; Ueda, N. The N-acylethanolamine-hydrolyzing acid amidase (NAAA). *Chem. Biodiversity* **2007**, *4*, 1914−1925.

(12) Piomelli, D.; Scalvini, L.; Fotio, Y.; Lodola, A.; Spadoni, G.; Tarzia, G.; Mor, M. N-acylethanolamine acid amidase: structure, function and inhibition. *J. Med. Chem.* **2020**, *63*, 7475−7490.

(13) Bracey, M. H.; Hanson, M. A.; Masuda, K. R.; Stevens, R. C.; Cravatt, B. F. Structural adaptations in a membrane enzyme that terminates endocannabinoid signaling. *Science* **2002**, *298*, 1793−1796.

(14) McKinney, M. K.; Cravatt, B. F. Structure and function of fatty acid amide hydrolase. *Annu. Rev. Biochem.* **2005**, *74*, 411−432.

(15) Patricelli, M. W.; Cravatt, B. F. Clarifying the catalytic roles of conserved residues in the amidase signature family. *J. Biol. Chem.* **2000**, *275*, 19177−19184.

(16) Brannigan, J. A.; Dodson, G.; Duggleby, H. J.; Moody, P. C.; Smith, J. L.; Tomchick, D. R.; Murzin, A. G. A protein catalytic framework with an N-terminal nucleophile is capable of self-activation. *Nature* **1995**, *378*, 416−419.

(17) Oinonen, C.; Rouvinen, J. Structural comparison of Ntn-hydrolases. *Protein Sci.* **2000**, *9*, 2329−2337.

(18) Zhao, L. Y.; Tsuboi, K.; Okamoto, Y.; Nagahata, S.; Ueda, N. Proteolytic activation and glycosylation of N-acylethanolamine-hydrolyzing acid amidase, a lysosomal enzyme involved in the endocannabinoid metabolism. *Biochim. Biophys. Acta, Mol. Cell Biol. Lipids* **2007**, *1771*, 1397−1405.

(19) Gorelik, A.; Gebai, A.; Illes, K.; Piomelli, D.; Nagar, B. Molecular mechanism of activation of the immunoregulatory amidase NAAA. *Proc. Natl. Acad. Sci. U. S. A.* **2018**, *115*, E10032−E10040.

(20) Wang, J.; Zhao, L. Y.; Uyama, T.; Tsuboi, K.; Tonai, T.; Ueda, N. Amino acid residues crucial in pH regulation and proteolytic activation of N-acylethanolamine-hydrolyzing acid amidase. *Biochim. Biophys. Acta, Mol. Cell Biol. Lipids* **2008**, *1781*, 710−717.

(21) Gebai, A.; Gorelik, A.; Li, Z.; Illes, K.; Nagar, B. Structural basis for the activation of acid ceramidase. *Nat. Commun.* **2018**, *9*, 1621.

(22) (a) Lodola, A.; Mor, M.; Hermann, J. C.; Tarzia, G.; Piomelli, D.; Mulholland, A. J. QM/MM modelling of oleamide hydrolysis in fatty acid amide hydrolase (FAAH) reveals a new mechanism of nucleophile activation. *Chem. Commun.* **2005**, 4399−4401. (b) Tubert-Brohman, I.; Acevedo, O.; Jorgensen, W. L. Elucidation of hydrolysis mechanisms for fatty acid amide hydrolase and its lys142ala variant via QM/MM simulations. *J. Am. Chem. Soc.* **2006**, *128*, 16904−16913. (c) Palermo, G.; Rothlisberger, U.; Cavalli, A.; De Vivo, M. Computational insights into function and inhibition of fatty acid amide hydrolase. *Eur. J. Med. Chem.* **2015**, *91*, 15−26.

(23) (a) Warshel, A.; Levitt, M. Theoretical studies of enzymic reactions: dielectric, electrostatic and steric stabilization of the carbonium ion in the reaction of lysozyme. *J. Mol. Biol.* **1976**, *103*, 227−249. (b) Field, M. J.; Bash, P. A.; Karplus, M. A combined quantum mechanical and molecular mechanical potential for molecular dynamics simulations. *J. Comput. Chem.* **1990**, *11*, 700−733. (c) Senn, H. M.; Thiel, W. QM/MM methods for biomolecular systems. *Angew. Chem., Int. Ed.* **2009**, *48*, 1198−1229. (d) van der Kamp, M. W.; Mulholland, A. J. Combined quantum mechanics/molecular mechanics (QM/MM) methods in computational enzymology. *Biochemistry* **2013**, *52*, 2708−2728.

(24) Branduardi, D.; Gervasio, F. L.; Parrinello, M. From A to B in free energy space. *J. Chem. Phys.* **2007**, *126*, 054103.
(25) Harder, E.; Damm, W.; Maple, J.; Wu, C.; Reboul, M.; Xiang, J. Y.; Wang, L.; Lupyan, D.; Dahlgren, M. K.; Knight, J. L.; Kaus, J. W.; Cerutti, D.; Krilov, G.; Jorgensen, W. L.; Abel, R.; Friesner, R. A. OPLS3: a force field providing broad coverage of drug-like small molecules and proteins. *J. Chem. Theory Comput.* **2016**, *12*, 281−296.
(26) Debiec, K. T.; Cerutti, D. S.; Baker, L. R.; Gronenborn, A. M.; Case, D. A.; Chong, L. T. Further along the road less traveled: AMBER ff15ipq, an original protein force field built on a self-consistent physical model. *J. Chem. Theory Comput.* **2016**, *12*, 3926−3947.
(27) Wang, J.; Wolf, R. M.; Caldwell, J. W.; Kollman, P. A.; Case, D. A. Development and testing of a general AMBER force field. *J. Comput. Chem.* **2004**, *25*, 1157−1174.
(28) Jorgensen, W. L.; Chandrasekhar, J.; Madura, J. D.; Impey, R. W.; Klein, M. L. Comparison of simple potential functions for simulating liquid water. *J. Chem. Phys.* **1983**, *79*, 926−935.
(29) Case, D. A.; Betz, R. M.; Cerutti, D. S.; Cheatham, III, T. E.; Darden, T. A.; Duke, R. E.; Giese, T. J.; Gohlke, H.; Goetz, A. W.; Homeyer, N.; Izadi, S.; Janowski, P.; Kaus, J.; Kovalenko, A.; Lee, T. S.; LeGrand, S.; Li, P.; Lin, C.; Luchko, T.; Luo, R.; Madej, B.; Mermelstein, D.; Merz, K. M.; Monard, G.; Nguyen, H.; Nguyen, H. T.; Omelyan, I.; Onufriev, A.; Roe, D. R.; Roitberg, A.; Sagui, C.; Simmerling, C. L.; Botello-Smith, W. M.; Swails, J.; Walker, R. C.; Wang, J.; Wolf, R. M.; Wu, X.; Xiao, L.; Kollman, P. A. *AMBER 2016*; University of California: San Francisco, 2016.
(30) Gaus, M.; Cui, Q.; Elstner, M. DFTB3: Extension of the self-consistent-charge density-functional tight-binding method (SCC-DFTB). *J. Chem. Theory Comput.* **2011**, *7*, 931−948.
(31) (a) Seabra, G. d. M.; Walker, R. C.; Elstner, M.; Case, D. A.; Roitberg, A. E. Implementation of the SCC-DFTB method for hybrid QM/MM simulations within the Amber molecular dynamics package. *J. Phys. Chem. A* **2007**, *111*, 5655−5664. (b) Walker, R. C.; Crowley, M. F.; Case, D. A. The implementation of a fast and accurate QM/MM potential method in Amber. *J. Comput. Chem.* **2008**, *29*, 1019−1031.
(32) Elstner, M. The SCC-DFTB method and its application to biological systems. *Theor. Chem. Acc.* **2006**, *116*, 316−325.
(33) Gaus, M.; Lu, X.; Elstner, M.; Cui, Q. Parameterization of DFTB3/3OB for Sulfur and Phosphorus for chemical and biological applications. *J. Chem. Theory Comput.* **2014**, *10*, 1518−1537.
(34) Lodola, A.; Callegari, D.; Scalvini, L.; Rivara, S.; Mor, M. Design and SAR analysis of covalent inhibitors driven by hybrid QM/MM simulations. *Methods Mol. Biol.* **2020**, *2114*, 307−337.
(35) Kumar, S.; Rosenberg, J. M.; Bouzida, D.; Swendsen, R. H.; Kollman, P. A. Multidimensional free-energy calculations using the weighted histogram analysis method. *J. Comput. Chem.* **1995**, *16*, 1339−1350.
(36) Grossfield, A. *WHAM: the weighted histogram analysis method, ver. 2.0.9*; http://membrane.urmc.rochester.edu/wordpress/?page_id=126.
(37) Marcos-Alcalde, I.; Setoain, J.; Mendieta-Moreno, J. I.; Mendieta, J.; Gomez-Puertas, P. MEPSA: minimum energy pathway analysis for energy landscapes. *Bioinformatics* **2015**, *31*, 3853−3855.
(38) Olsson, M. H.; Søndergaard, C. R.; Rostkowski, M.; Jensen, J. H. PROPKA3: Consistent treatment of internal and surface residues in empirical pKa predictions. *J. Chem. Theory Comput.* **2011**, *7*, 525−537.
(39) Elsässer, B.; Zauner, F. B.; Messner, J.; Soh, W. T.; Dall, E.; Brandstetter, H. Distinct roles of catalytic cysteine and histidine in the protease and ligase mechanisms of human legumain as revealed by DFT-based QM/MM simulations. *ACS Catal.* **2017**, *7*, 5585−5593.
(40) Lodola, A.; Branduardi, D.; De Vivo, M.; Capoferri, L.; Mor, M.; Piomelli, D.; Cavalli, A. A catalytic mechanism for cysteine N-terminal nucleophile hydrolases, as revealed by free energy simulations. *PLoS One* **2012**, *7*, e32397.
(41) Ma, S.; Devi-Kesavan, L. S.; Gao, J. Molecular dynamics simulations of the catalytic pathway of a cysteine protease: a combined QM/MM study of human cathepsin K. *J. Am. Chem. Soc.* **2007**, *129*, 13633−13645.
(42) Arafet, K.; Ferrer, S.; Moliner, V. Computational study of the catalytic mechanism of the cruzain cysteine protease. *ACS Catal.* **2017**, *7*, 1207−1215.
(43) Syrén, P. O. The solution of nitrogen inversion in amidases. *FEBS J.* **2013**, *280*, 3069−3083.
(44) Mujika, J. I.; Formoso, E.; Mercero, J. M.; Lopez, X. Reaction mechanism of the acidic hydrolysis of highly twisted amides: Rate acceleration caused by the twist of the amide bond. *J. Phys. Chem. B* **2006**, *110*, 15000−15011.
(45) Lodola, A.; Capoferri, L.; Rivara, S.; Tarzia, G.; Piomelli, D.; Mulholland, A.; Mor, M. Quantum mechanics/molecular mechanics modeling of fatty acid amide hydrolase reactivation distinguishes substrate from irreversible covalent inhibitors. *J. Med. Chem.* **2013**, *56*, 2500−2512.
(46) (a) Lodola, A.; Mor, M.; Sirirak, J.; Mulholland, A. J. Insights into the mechanism and inhibition of fatty acid amide hydrolase from quantum mechanics/molecular mechanics (QM/MM) modelling. *Biochem. Soc. Trans.* **2009**, *37*, 363−367. (b) Palermo, G.; Campomanes, P.; Cavalli, A.; Rothlisberger, U.; De Vivo, M. Anandamide hydrolysis in FAAH reveals a dual strategy for efficient enzyme-assisted amide bond cleavage via nitrogen inversion. *J. Phys. Chem. B* **2015**, *119*, 789−801.
(47) Cho, S. J.; Cui, C.; Lee, J. Y.; Park, J. K.; Suh, S. B.; Park, J.; Kim, B. H.; Kim, K. S. N-Protonation vs O-Protonation in Strained Amides: Ab Initio Study. *J. Org. Chem.* **1997**, *62*, 4068−4071.
(48) Aubè, J. A new twist on amide solvolysis. *Angew. Chem., Int. Ed.* **2012**, *51*, 3063−305.
(49) Ekici, O. D.; Paetzel, M.; Dalbey, R. E. Unconventional serine proteases: variations on the catalytic Ser/His/Asp triad configuration. *Protein Sci.* **2008**, *17*, 2023−2037.
(50) Gruden, M.; Andjeklović, L.; Jissy, A. K.; Stepanović, S.; Zlatar, M.; Cui, Q.; Elstner, M. Benchmarking density functional tight binding models for barrier heights and reaction energetics of organic molecules. *J. Comput. Chem.* **2017**, *38*, 2171−2185.
(51) Awoonor-Williams, E.; Isley, W. C., 3rd; Dale, S. G.; Johnson, E. R.; Yu, H.; Becke, A. D.; Roux, B.; Rowley, C. N. Quantum chemical methods for modeling covalent modification of biological thiols. *J. Comput. Chem.* **2020**, *41*, 427−438.
(52) Hirvonen, V. H. A.; Mulholland, A. J.; Spencer, J.; van der Kamp, M. W. Small changes in hydration determine cephalosporinase activity of OXA-48 β-lactamases. *ACS Catal.* **2020**, *10*, 6188−6196.
(53) Silva, J. R. A.; Cianni, L.; Araujo, D.; Batista, P. H. J.; de Vita, D.; Rosini, F.; Leitão, A.; Lameira, J.; Montanari, C. A. Assessment of the Cruzain cysteine protease reversible and irreversible covalent inhibition mechanism. *J. Chem. Inf. Model.* **2020**, *60*, 1666−1677.
(54) (a) Duranti, A.; Tontini, A.; Antonietti, F.; Vacondio, F.; Fioni, A.; Silva, C.; Lodola, A.; Rivara, S.; Solorzano, C.; Piomelli, D.; Tarzia, G.; Mor, M. N-(2-Oxo-3-oxetanyl)carbamic acid esters as N-acylethanolamine acid amidase inhibitors: synthesis and structure−activity and structure−property relationships. *J. Med. Chem.* **2012**, *55*, 4824−4836. (b) Ponzano, S.; Berozzi, F.; Mengatto, L.; Dionisi, M.; Armirotti, A.; Romeo, E.; Berteotti, A.; Fiorelli, C.; Tarozzo, G.; Reggiani, A.; Duranti, A.; Tarzia, G.; Mor, M.; Cavalli, A.; Piomelli, D.; Bandiera, T. Synthesis and structure−activity relationship (SAR) of 2-methyl-4-oxo-3-oxetanylcarbamic acid esters, a class of potent N-acylethanolamine acid amidase (NAAA) inhibitors. *J. Med. Chem.* **2013**, *56*, 6917−6934.
(55) Fiasella, A.; Nuzzi, A.; Summa, M.; Armirotti, A.; Tarozzo, G.; Tarzia, G.; Mor, M.; Bertozzi, F.; Bandiera, T.; Piomelli, D. 3-Aminoazetidin-2-one derivatives as N-acylethanolamine acid amidase (NAAA) inhibitors suitable for systemic administration. *ChemMedChem* **2014**, *9*, 1602−1614. (b) Ribeiro, A.; Pontis, S.; Mengatto, L.; Armirotti, A.; Chiurchiù, V.; Capurro, V.; Fiasella, A.; Nuzzi, A.; Romeo, E.; Moreno-Sanz, G.; Maccarrone, M.; Reggiani, A.; Tarzia, G.; Mor, M.; Bertozzi, F.; Bandiera, T.; Piomelli, D. A potent systemically active N-acylethanolamine acid amidase inhibitor that suppresses inflammation and human macrophage activation. *ACS*

Chem. Biol. **2015**, *10*, 1838−1846. (c) Nuzzi, A.; Fiasella, A.; Ortega, J. A.; Pagliuca, C.; Ponzano, S.; Pizzirani, D.; Bertozzi, S. M.; Ottonello, G.; Tarozzo, G.; Reggiani, A.; Bandiera, T.; Bertozzi, F.; Piomelli, D. Potent α-amino-β-lactam carbamic acid ester as NAAA inhibitors. Synthesis and structure-activity relationship (SAR) studies. *Eur. J. Med. Chem.* **2016**, *111*, 138−159. (d) Petracca, R.; Ponzano, S.; Bertozzi, S. M.; Sasso, O.; Piomelli, D.; Bandiera, T.; Bertozzi, F. Progress in the development of β-lactams as N-acylethanolamine acid amidase (NAAA) inhibitors: synthesis and SAR study of new, potent N-O-substituted derivatives. *Eur. J. Med. Chem.* **2017**, *126*, 561−575.

(56) Armirotti, A.; Romeo, E.; Ponzano, S.; Mengatto, L.; Dionisi, M.; Karacsonyi, C.; Bertozzi, F.; Garau, G.; Tarozzo, G.; Reggiani, A.; Bandiera, T.; Tarzia, G.; Mor, M.; Piomelli, D. β-Lactones inhibit N-acylethanolamine acid amidase by S-acylation of the catalytic N-terminal cysteine. *ACS Med. Chem. Lett.* **2012**, *3*, 422−426.

(57) Chilov, G. G.; Sidorova, A. V.; Svedas, V. K. Quantum chemical studies of the catalytic mechanism of N-terminal nucleophile hydrolase. *Biochemistry (Moscow)* **2007**, *72*, 495−500.

(58) Perakyla, M.; Rouvinen, J. Ab Initio quantum mechanical model calculations on the catalytic mechanism of aspartylglucosaminidase (AGA): a serine protease-like mechanism with an N-terminal threonine and substrate-assisted catalysis. *Chem. - Eur. J.* **1996**, *2*, 1548−1551.

(59) Khavrutskii, I. V.; Legler, P. M.; Friedlander, A. M.; Wallqvist, A. A reaction path study of the catalysis and inhibition of the Bacillus anthracis CapD γ-glutamyl transpeptidase. *Biochemistry* **2014**, *53*, 6954−6967.

https://dx.doi.org/10.1021/acscatal.0c02903
ACS Catal. 2020, 10, 11797−11813